

**SECOND-ORDER CONE PROGRAMMING BASED METHODS  
FOR TWO VARIANTS OF OPTIMAL POWER FLOW**

by  
SEZEN ECE KAYACIK

Submitted to the Graduate School of Engineering and Natural Sciences  
in partial fulfilment of  
the requirements for the degree of Master of Science

Sabanci University  
August 2020

**SECOND-ORDER CONE PROGRAMMING BASED METHODS  
FOR TWO VARIANTS OF OPTIMAL POWER FLOW**

Approved by:

Asst. Prof. BURAK KOCUK .....  
(Thesis Supervisor)

Asst. Prof. TUĞÇE YÜKSEL .....  
(Thesis Co-Supervisor)

Asst. Prof. BESTE BAŞÇİFTÇİ .....

Prof. TONGUÇ ÜNLÜYURT .....

Assoc. Prof. MURAT GÖL .....

Date of Approval: August 18, 2020

THESIS AUTHOR 2020 ©

All Rights Reserved

## ABSTRACT

### SECOND-ORDER CONE PROGRAMMING BASED METHODS FOR TWO VARIANTS OF OPTIMAL POWER FLOW

SEZEN ECE KAYACIK

INDUSTRIAL ENGINEERING M.S. THESIS, 2020

Thesis Supervisor: Assist. Prof. BURAK KOCUK  
Thesis Co-Supervisor: Asst. Prof. TUĞÇE YÜKSEL

Keywords: reactive optimal power flow, second-order cone programming  
mixed-integer nonlinear programming, multi-period optimal power flow

Optimal Power Flow (OPF) is a fundamental optimization problem in power system operations. In this thesis, we focus on two variants of the OPF problem: Reactive Optimal Power Flow (ROPF) and Multi-Period Optimal Power Flow (MOPF). In Chapter 2, we provide an overview of the classical OPF formulations. In Chapter 3, we present an alternative mixed-integer non-linear programming formulation of the ROPF problem. We utilize a mixed-integer second-order cone programming (MISOCP) based approach to find globally optimal solutions of the proposed ROPF problem formulation. We strengthen the MISOCP relaxation via the addition of convex envelopes and cutting planes. Computational experiments on challenging test cases show that the MISOCP-based approach yields promising results with small optimality gaps compared to a semidefinite programming based approach from the literature. In Chapter 4, we focus on the MOPF problem with electric vehicles (EV) under emission considerations. Our model integrates three different real data sets: household electricity consumption, marginal emission factors, and EV driving profiles. We present a systematic solution approach based on SOCP to find globally optimal solutions. Our computational experiments on instances with up to 2000 buses demonstrate that our solution approach leads to globally optimal solutions with very small optimality gaps, in addition to significant emission savings and reductions in cost with the coordination of EV charging.

## ÖZET

### ENIYI GÜÇ AKIŞI PROBLEMİNİN İKİ SÜRÜMÜ İÇİN İKİNCİ DERECEDEN KONİK PROGRAMLAMA TEMELLİ YÖNTEMLER

SEZEN ECE KAYACIK

ENDÜSTRİ MÜHENDİSLİĞİ YÜKSEK LİSANS TEZİ, 2020

Tez Danışmanı: Dr. BURAK KOCUK

Eş Tez Danışmanı: Dr. TUĞÇE YÜKSEL

Anahtar Kelimeler: reaktif eniyi güç akışı, ikinci dereceden konik programlama, karma tamsayı doğrusal olmayan programlama, çok periyotlu eniyi güç akışı

Bu tezde eniyi güç akışı probleminin iki farklı sürümü olan reaktif eniyi güç akışı problemi ve çok periyotlu eniyi güç akışı problemi çalışılmıştır. Bölüm 2’de, klasik eniyi güç akışı problemine genel bir bakış sunulmuştur. Bölüm 3’te, reaktif eniyi güç akışı problemi için alternatif bir karma tamsayı doğrusal olmayan programlama modeli kurulmuştur. Modelin küresel eniyi çözümünü bulmak için karma tamsayı ikinci dereceden konik programlama yönteminden yararlanılmıştır. Dışbükey zarflar ve kesen düzlemler ile birlikte bu yaklaşım güçlendirilmiştir. Önerilen yöntemin sonuçları literatürdeki bir yarı belirli programlama temelli yaklaşımın sonuçları ile karşılaştırıldığında zor test vakaları üzerinde yeterince iyi sonuçlar alınmıştır. Bölüm 4’te, elektrikli araçları ve oluşturdukları emisyonu da dahil ederek çok periyotlu eniyi güç akışı problemi üzerinde çalışılmıştır. Problemin modeli ev içi elektrik tüketimi, marjinal emisyon faktörleri ve elektrikli araç sürüş profilleri olmak üzere üç farklı gerçek veri setini içermektedir. Bu problem için de küresel eniyi çözümler elde edebilmek için ikinci dereceden konik programlamaya dayalı sistematik bir çözüm yaklaşımı sunulmuştur. İki bine kadar düğümü olan ağlar üzerinde yapılan deneyler, sunulan yaklaşımın çok küçük eniyilik açığı olan küresel eniyi çözümlere ulaştığını göstermektedir. Buna ek olarak deney sonuçları elektrikli araçların koordineli bir şekilde şarj edilmesi ile emisyonun ciddi derecede azaltılabileceğini ve üretim maliyetlerinde de azalma sağlanabileceğini göstermektedir.

## TABLE OF CONTENTS

<b>LIST OF TABLES</b> .....	<b>viii</b>
<b>LIST OF FIGURES</b> .....	<b>ix</b>
<b>NOMENCLATURE</b> .....	<b>x</b>
<b>1. INTRODUCTION</b> .....	<b>1</b>
<b>2. OPTIMAL POWER FLOW PROBLEM</b> .....	<b>3</b>
2.1. Literature Review .....	3
2.2. Formulations .....	5
2.2.1. Rectangular Formulation .....	5
2.2.2. Polar Formulation .....	6
2.2.3. Alternative Formulation.....	7
2.2.4. Relaxations .....	8
<b>3. REACTIVE OPTIMAL POWER FLOW PROBLEM</b> .....	<b>9</b>
3.1. Literature Review .....	9
3.2. Formulations .....	10
3.2.1. Alternative .....	11
3.2.2. MISOCP Relaxation .....	14
3.2.3. Tightened MISOCP Relaxation .....	14
3.3. Solution Approach .....	16
3.4. Computational Experiments .....	16
3.4.1. The Effect of Tap Ratio Discretization .....	19
3.4.2. A Test Case for a Larger Instance .....	19
3.5. Conclusions .....	20
<b>4. MULTI-PERIOD OPTIMAL POWER FLOW PROBLEM WITH ELECTRIC VEHICLES</b> .....	<b>21</b>
4.1. Introduction .....	21
4.1.1. Literature Review .....	22

4.1.2. Contributions .....	24
4.2. Formulations .....	25
4.2.1. Alternative Formulation.....	27
4.2.2. SOCP Relaxations .....	28
4.3. Solution Approach .....	29
4.4. Input.....	30
4.4.1. OPF Test Case.....	30
4.4.2. Electricity Demand.....	31
4.4.3. Emission Factors .....	33
4.4.4. Driving Profiles .....	33
4.5. Computational Experiments .....	35
4.5.1. Experimental Setup .....	35
4.5.2. Results and Discussion .....	38
4.5.2.1. Computational Accuracy in Terms of Optimality Gap .....	39
4.5.2.2. Marginal Cost vs. Marginal Emission .....	40
4.5.2.3. Effect of V2G.....	40
4.5.2.4. Hourly Load Variations for Illinois 200-Bus System ..	47
4.6. Conclusions .....	50
<b>BIBLIOGRAPHY.....</b>	<b>51</b>

## LIST OF TABLES

Table 3.1. Computational results with 0.0125 discretization step size. Instances with the SOCP optimality gap above 3% are indicated with an asterisk. ....	17
Table 3.2. Computational results with 0.05 discretization step size. Instances with the SOCP optimality gap above 3% are indicated with an asterisk. ....	18
Table 4.1. Size of the instances. ....	31
Table 4.2. Daily demands in kWh. ....	38
Table 4.3. Input data and parameter settings. ....	39



## LIST OF FIGURES

Figure 4.1. Hourly electricity demand. ....	32
Figure 4.2. Marginal CO <sub>2</sub> emission factors. ....	33
Figure 4.3. Percentage of energy requirement of EVs by time of day. ....	35
Figure 4.4. Pareto frontier of total cost and marginal emission for Illinois (200-bus system) in winter. ....	41
Figure 4.5. Pareto frontier of marginal cost and marginal emission for Illinois (200-bus system) in winter. ....	41
Figure 4.6. Pareto frontier of total cost and marginal emission for Illinois (200-bus system) in summer. ....	42
Figure 4.7. Pareto frontier of marginal cost and marginal emission for Illinois (200-bus system) in summer. ....	42
Figure 4.8. Pareto frontier of total cost and marginal emission for South Carolina (500-bus system) in winter. ....	43
Figure 4.9. Pareto frontier of marginal cost and marginal emission for South Carolina (500-bus system) in winter. ....	43
Figure 4.10. Pareto frontier of total cost and marginal emission for South Carolina (500-bus system) in summer. ....	44
Figure 4.11. Pareto frontier of marginal cost and marginal emission for South Carolina (500-bus system) in summer. ....	44
Figure 4.12. Pareto frontier of total cost and marginal emission for Texas (2000-bus system) in winter. ....	45
Figure 4.13. Pareto frontier of marginal cost and marginal emission for Texas (2000-bus system) in winter. ....	45
Figure 4.14. Pareto frontier of total cost and marginal emission for Texas (2000-bus system) in summer. ....	46
Figure 4.15. Pareto frontier of marginal cost and marginal emission for Texas (2000-bus system) in winter. ....	46
Figure 4.16. Hourly load variations for Illinois (200-bus system) in winter.	48
Figure 4.17. Hourly load variations for Illinois (200-bus system) in summer.	49

## NOMENCLATURE

$\delta(i)$	Set of neighbors of bus $i$
$\eta_i$	Charging efficiency of EV for bus $i$
$\bar{S}_{ij}$	Apparent flow limit for line $(i, j)$
$\bar{\theta}_{ij}$	Bound on the phase angle of line $(i, j)$
$\bar{a}_{it}, \bar{b}_{it}$	Maximum allowable charging and discharging rates of EV for bus $i$ at time $t$
$\bar{E}$	Upper bound on the total $CO_2$ emission
$\tau_{ij}$	Tap ratio of line $(i, j)$
$\tau_{ij}^l$	Allowable tap ratio $l$ for line $(i, j)$
$\underline{V}_i, \bar{V}_i$	Upper and lower bounds on the voltage magnitude of bus $i$
$\underline{p}_i, \bar{p}_i$	Upper and lower bounds on the real output of generator $i$
$\underline{q}_i, \bar{q}_i$	Upper and lower bounds on the reactive output of generator $i$
$\underline{s}_{it}, \bar{s}_{it}$	Minimum energy requirement and maximum capacity of EV battery for bus $i$ at time $t$
$b_{ii}^k$	Allowable shunt susceptance $k$ for bus $i$
$B_{ij}, B_{ji}$	Susceptance of line $(i, j)$
$c_{it}$	Energy requirement of EV for bus $i$ at time $t$
$e_t$	Marginal emission parameter at time $t$
$g_{ii}$	Shunt susceptance of bus $i$

$g_{ii}, b_{ii}$  Shunt susceptance of bus  $i$   
 $G_{ij}, G_{ji}$  Conductance of line  $(i, j)$   
 $I_i$  Initial battery state of charge of EV for bus  $i$   
 $L_i, Q_i$  Linear and quadratic costs of generator  $i$   
 $p_{it}^d, q_{it}^d$  Real and reactive power load of bus  $i$  at time  $t$   
 $p_i^d, q_i^d$  Real and reactive power load of bus  $i$   
 $\alpha_i^k$   $\alpha_i^k = 1$  if  $b_{ii} = b_{ii}^k$ , and 0 otherwise for bus  $i$   
 $\beta_{ij}^l$   $\beta_{ij}^l = 1$  if  $\tau_{ij} = \tau_{ij}^l$ , and 0 otherwise for line  $(i, j)$   
 $\tau_{ij}$  Tap ratio of line  $(i, j)$   
 $\theta_{it}$  Phase angle of bus  $i$  at time  $t$   
 $\theta_i$  Phase angle of bus  $i$   
 $a_{it}, b_{it}$  Charging and discharging power of EV for bus  $i$  at time  $t$   
 $b_{ii}$  Shunt susceptance of bus  $i$   
 $p_{ijt}, q_{ijt}$  Real and reactive power flow of line  $(i, j)$  at time  $t$   
 $p_{ij}, q_{ij}$  Real and reactive power flow of line  $(i, j)$   
 $p_{it}^g, q_{it}^g$  Real and reactive power output of generator  $i$  at time  $t$   
 $p_i^g, q_i^g$  Real and reactive power output of generator  $i$   
 $s_{it}$  Stock variable of EV for bus  $i$  at time  $t$   
 $V_{it}$  Voltage of bus  $i$  at time  $t$   
 $V_i$  Voltage of bus  $i$

## 1. INTRODUCTION

Power systems is concerned with generating, transmitting, and distributing electricity through networks so as to deliver electricity to consumers. Optimal Power Flow (OPF) has been one of the most widely studied and important problems in the area of power systems. OPF determines the optimal operations of the power network while satisfying the power flow equations and network constraints, meeting operation feasibility and security. Within this framework, a huge variety of OPF formulations and solution strategies have been presented.

The general OPF formulation is highly nonconvex, and therefore developing both efficient and accurate algorithms is usually challenging. In recent years, convex relaxations of the OPF problem have drawn a substantial research interest since they can provide the guarantee of global optimality or convergence. In this thesis, we focus on two variants of the OPF problem and propose SOCP-based solution approaches, aiming to find globally optimal solutions. The first problem is the reactive optimal power flow (ROPF) which contains discrete control variables such as shunt susceptance and tap ratio. The ROPF problem is generally more challenging to solve than the OPF due to the presence of these discrete variables.

The second problem is multi-period optimal power flow (MOPF). The nature of OPF is rapidly evolving with the integration of new technologies into the network, such as electric vehicles, and network operations will become more challenging. Therefore, the large scale integration of electric vehicles brings the necessity of solving MOPF problem to coordinate charging strategies efficiently. The MOPF problem optimizes operations of the power grid with respect to a certain objective and network constraints over a finite planning horizon.

The remainder of the thesis is organized as follows. In Chapter 2, we review the literature on the classical OPF problem and its formulations. In Chapter 3, we focus on developing a systematic approach for solving the ROPF problem. In Chapter 4, we propose a mathematical formulation of MOPF with electric vehicles (EV) under emission considerations and investigate the effects of EV charging loads on

the optimal operations of the distribution network.

## 2. OPTIMAL POWER FLOW PROBLEM

### 2.1 Literature Review

The optimal power flow (OPF) problem is one of the major tools to find optimal power system operations while satisfying the power flow equations and network constraints, meeting operation feasibility and security. Since introduced by Carpentier (1962), a wide variety of solution methods have been presented such as Nonlinear Programming (NLP), Quadratic Programming (QP), Interior point methods (IPM) and heuristic algorithms. The problem formulation includes nonconvex and nonlinear functions. Therefore, one might experience issues such as converging to a locally optimal solution or an infeasible point while solving large scale OPF problems. Recently, convex relaxations that can overcome these difficulties appeared in the literature and have drawn significant research interest. In subsequent paragraphs, we discuss the previous studies together with their advantages and disadvantages.

NLP-based solution methods relying on the Karush–Kuhn–Tucker (KKT) conditions are among the first attempts to solve the OPF problem. For example, Shen & Laughton (1969) implement an iterative indirect approach based on the KKT conditions on a small size system. El-Abiad & Jaimes (1969) present a similar approach for the OPF problem using an acceleration factor to improve convergence. The paper by Sasson, Vilorio & Aboytes (1973) proposes the first method that exploits the sparsity of the Hessian matrix for solving the OPF problem; however, it does not work well with the reactive part of the problem. Sun, Ashley, Brewer, Hughes & Tinney (1984) solve the OPF problem using an explicit Newton approach. The challenging part of this approach is identifying the binding constraints. Once the set of binding constraints is known, the algorithm converges the optimal solution within a few iterations.

Santos & Da Costa (1995) present the Dual-Newton approach in which the binding constraints are not needed to be known, and the equality constraints are handled with Lagrange multipliers. However, insecure convergence and algorithmic complexity are the potential disadvantages of these NLP based methods (Soliman & Mantawy, 2011).

The nonlinear solution approaches are also presented in a decomposed manner to improve the computation time and simplify the OPF formulation. Shoultz & Sun (1982) decompose the OPF problem into two subproblems: one corresponds to real power optimization assuming voltages are constant and the other to reactive power optimization assuming real power generation and phase angles are constant. Jolis-saint, Arvanitidis & Luenberger (1972) suggest a similar decomposition approach, where subproblems are alternatively solved with the use of successive linear programming.

Another class of optimization methods for OPF uses IPM, which has appealing features easily handling the inequality constraints and converging speed (Capitanescu, Glavic, Ernst & Wehenkel, 2007). In Jabr, Coonick & Cory (2002), the authors focus on enhancing the convergence properties of the IPMs controlling search direction and step length with the use of a filter technique. Chiang, Wang & Jiang (2009) develop an algorithm to improve initial starting conditions. Moyano & Salgado (2010) present a parameterized formulation to solve the issue of divergence when the model is infeasible. However, similar to the other nonlinear optimization methods, the IPM's major drawback is that it does not guarantee to converge to a globally optimal solution because of the nonconvexity of the OPF problem.

Heuristic optimization algorithms to solve the OPF problem have also been discussed in the literature. There are several examples of these heuristics such as genetic algorithm (Paranjothi & Anburaja, 2002), tabu search (Ongsakul & Tantimaporn, 2006), particle swarm optimization (Abido, 2002), simulated annealing (Roa-Sepulveda & Pavez-Lazo, 2003) and hybrid heuristic algorithms. A comprehensive overview of these algorithms can be found in Frank, Steponavice & Rebennack (2012). The main drawback of a heuristic algorithm is its possible convergence to locally optimal solutions, which is highly dependent on the initial starting point. Also, heuristics are built based on several theoretical assumptions such as differentiability and convexity that do not always hold for the actual OPF conditions (AlRashidi & El-Hawary, 2009).

In Bukhsh, Grothey, McKinnon & Trodden (2013), the authors point out that locally optimal OPF solutions exist in several test cases, which brings the necessity of using an efficient algorithm to obtain a globally optimal solution. Therefore, recent

studies have focused on convex programming methods to certify global optimality. The paper by Bai, Wei, Fujisawa & Wang (2008) uses quadratically constrained quadratic OPF formulation in order to convert it into a semidefinite programming (SDP) problem. Jabr (2011) and Molzahn, Holzer, Lesieutre & DeMarco (2013) make use of sparsity in SDP relaxations to decrease the computational effort. A second-order cone programming relaxation of the OPF problem is first introduced in Jabr (2006), and its exactness is discussed in Gan, Li, Topcu & Low (2014). Other convex relaxation methods such as convex dist-flow (Farivar, Clarke, Low & Chandy, 2011), moment-based (Molzahn & Hiskens, 2014) and quadratic convex (Coffrin, Hijazi & Van Hentenryck, 2015b) have also been proposed in the literature. Kocuk, Dey & Sun (2016) propose strengthened SOCP relaxations which perform better than the other convex relaxations and competitive against SDP relaxations in terms of solution quality. In a subsequent study (Kocuk, Dey & Sun, 2018), with the use of some techniques such as cutting planes and convex envelopes, they further strengthen the SOCP relaxation and propose a method that outperforms the standard SDP relaxation.

## 2.2 Formulations

In this section, we will provide formulations of the OPF problem involving Alternating Current (AC) power flow equations. Consider a power network  $\mathcal{N} = (\mathcal{B}, \mathcal{L})$ , where  $\mathcal{B}$  denotes the node set, i.e., the set of buses, and  $\mathcal{L}$  denotes the edge set, i.e., the set of transmission lines. Let  $\mathcal{G} \subseteq \mathcal{B}$  denote the set of generators attached to a subset of buses. We list the parameters and decision variables needed for the formulations in nomenclature.

### 2.2.1 Rectangular Formulation

In the AC OPF formulation, the voltage  $V_i$  at bus  $i \in \mathcal{B}$  is defined as a complex number. In the rectangular formulation, the complex bus voltage is expressed by  $V_i = e_i + if_i$  where  $e_i$  and  $f_i$  are the real and imaginary components, respectively. The



rectangular formulation of the OPF problem is given as follows:

$$\begin{aligned}
(2.1a) \quad & \min \sum_{i \in \mathcal{G}} h(p_i^g) \\
(2.1b) \quad & \text{s.t. } p_i^g - p_i^d = g_{ii}(e_i^2 + f_i^2) + \sum_{j \in \delta(i)} p_{ij} & i \in \mathcal{B} \\
(2.1c) \quad & q_i^g - q_i^d = -b_{ii}(e_i^2 + f_i^2) + \sum_{j \in \delta(i)} q_{ij} & i \in \mathcal{B} \\
(2.1d) \quad & p_{ij} = G_{ij}(e_i^2 + f_i^2) + G_{ij}(e_i e_j + f_i f_j) - B_{ij}(e_i f_j - e_j f_i) & (i, j) \in \mathcal{L} \\
(2.1e) \quad & q_{ij} = -B_{ij}(e_i^2 + f_i^2) - B_{ij}(e_i e_j + f_i f_j) + G_{ij}(e_i f_j - e_j f_i) & (i, j) \in \mathcal{L} \\
(2.1f) \quad & \underline{V}_i^2 \leq e_i^2 + f_i^2 \leq \bar{V}_i^2 & i \in \mathcal{B} \\
(2.1g) \quad & |\text{atan2}(f_i/e_i) - \text{atan2}(f_j/e_j)| \leq \bar{\theta}_{ij} & (i, j) \in \mathcal{L} \\
(2.1h) \quad & p_{ij}^2 + q_{ij}^2 \leq \bar{S}_{ij}^2 & (i, j) \in \mathcal{L} \\
(2.1i) \quad & \underline{p}_i \leq p_i^g \leq \bar{p}_i & i \in \mathcal{G} \\
(2.1j) \quad & \underline{q}_i \leq q_i^g \leq \bar{q}_i & i \in \mathcal{G}.
\end{aligned}$$

Here, the objective function (2.1a) minimizes the total power generation cost. Constraints (2.1b)–(2.1c) derived from Kirchhoff’s Current Law enforce the real and reactive power flow balance at bus  $i$ . Constraints (2.1d)–(2.1e) derived from Kirchhoff’s Voltage Law correspond to real and reactive power flow at line  $(i, j)$ . Constraint (2.1f) represent the limits associated with voltage magnitude at bus  $i$ . Constraint (2.1g)–(2.1h) restrict the phase angle and the apparent flow at line  $(i, j)$ . Constraints (2.1i)–(2.1j) set the upper and lower bounds on the real and reactive power output of generator  $i$ . Also, we set  $\underline{p}_i = \bar{p}_i = \underline{q}_i = \bar{q}_i = 0$  for  $i \in \mathcal{B} \setminus \mathcal{G}$ .

Using rectangular formulation when applying IPMs may provide an advantage as the Hessian matrix of the quadratic equations is constant (Sun & Phan, 2011). In addition, since the trigonometric terms are not involved, the computational complexity reduces. For instance, in Torres & Quintana (1998) and Capitanescu et al. (2007) rectangular formulation is utilized in the application of the IPM to OPF problem.

## 2.2.2 Polar Formulation

In the polar formulation, bus voltages are expressed by voltage magnitude  $|V_i|$  and phase angle  $\theta_i$  as follow:  $V_i = |V_i|(\cos(\theta_i) + i \sin(\theta_i))$ .

The OPF problem can be equivalently modeled in polar coordinates as follows:

$$\begin{aligned}
(2.2a) \quad & \min \sum_{i \in \mathcal{G}} h(p_i^g) \\
(2.2b) \quad & \text{s.t. } p_i^g - p_i^d = g_{ii}|V_i|^2 + \sum_{j \in \delta(i)} p_{ij} \quad i \in \mathcal{B} \\
(2.2c) \quad & q_i^g - q_i^d = -b_{ii}|V_i|^2 + \sum_{j \in \delta(i)} q_{ij} \quad i \in \mathcal{B} \\
(2.2d) \quad & p_{ij} = G_{ij}|V_i|^2 + |V_i||V_j|[G_{ij} \cos(\theta_i - \theta_j) - B_{ij} \sin(\theta_i - \theta_j)] \quad (i, j) \in \mathcal{L} \\
(2.2e) \quad & q_{ij} = -B_{ij}|V_i|^2 - |V_i||V_j|[B_{ij} \cos(\theta_i - \theta_j) + G_{ij} \sin(\theta_i - \theta_j)] \quad (i, j) \in \mathcal{L} \\
(2.2f) \quad & \underline{V}_i \leq |V_i| \leq \bar{V}_i \quad i \in \mathcal{B} \\
(2.2g) \quad & |\theta_i - \theta_j| \leq \bar{\theta}_{ij} \quad (i, j) \in \mathcal{L} \\
& (2.1h)-(2.1j).
\end{aligned}$$

Here, the quadratic equality constraints in (2.1) replaced with the polar formulations. Now the nonlinear quadratic voltage constraint (2.1f) and phase angle constraint (2.1g) that includes trigonometric function turn into linear constraints. One can take advantage of using linear voltage constraints in the case where the voltage magnitude of certain buses is given. In this particular case, the number of decision variables decreases in the polar formulation, while the number of quadratic equality constraints increases in the rectangular formulation (Sun & Phan, 2011).

The literature mostly uses the polar formulation while the rectangular formulation is included in a smaller number of papers (Cain, O'neill & Castillo, 2012). However, one can easily convert an optimal solution of the polar formulation into an optimal solution of the rectangular formulation and vice versa.

### 2.2.3 Alternative Formulation

Now we provide the alternative formulation first introduced in Expósito & Ramos (1999). Let us define a set of new variables  $c_{ii}$ ,  $c_{ij}$  and  $s_{ij}$ , respectively representing the quantities  $|V_i|^2$ ,  $|V_i||V_j|\cos(\theta_i - \theta_j)$  and  $-|V_i||V_j|\sin(\theta_i - \theta_j)$  for  $i \in \mathcal{B}$  and  $(i, j) \in \mathcal{L}$ , respectively. By replacing these new decision variables, the alternative formulation is obtained as follows:

$$(2.3a) \quad \min \sum_{i \in \mathcal{G}} h(p_i^g)$$

$$\begin{aligned}
(2.3b) \quad & \text{s.t. } p_i^g - p_i^d = g_{ii}c_{ii} + \sum_{j \in \delta(i)} p_{ij} & i \in \mathcal{B} \\
(2.3c) \quad & q_i^g - q_i^d = -b_{ii}c_{ii} + \sum_{j \in \delta(i)} q_{ij} & i \in \mathcal{B} \\
(2.3d) \quad & p_{ij} = G_{ij}c_{ii} + G_{ij}c_{ij} - B_{ij}s_{ij} & (i, j) \in \mathcal{L} \\
(2.3e) \quad & q_{ij} = -B_{ij}c_{ii} - B_{ij}c_{ij} - G_{ij}s_{ij} & (i, j) \in \mathcal{L} \\
(2.3f) \quad & \underline{V}_i^2 \leq c_{ii} \leq \overline{V}_i^2 & i \in \mathcal{B} \\
(2.3g) \quad & c_{ij}^2 + s_{ij}^2 = c_{ii}c_{jj} & (i, j) \in \mathcal{L} \\
(2.3h) \quad & \theta_j - \theta_i = \text{atan2}(s_{ij}, c_{ij}) & (i, j) \in \mathcal{L} \\
& (2.2g), (2.1h)-(2.1j).
\end{aligned}$$

Constraints (2.3g) and (2.3h) are the consistency constraints that preserve the trigonometric relation between the variables  $c_{ii}, c_{ij}$  and  $s_{ij}$ .

#### 2.2.4 Relaxations

The alternative formulation consist of convex constraints except (2.3g) and (2.3h). To convexify feasible region of the problem (2.3), we relax the constraint (2.3g) as a second-order cone constraint and eliminate constraint (2.3h). The SOCP relaxation of the alternative formulation is given as:

$$\begin{aligned}
(2.4a) \quad & \min \sum_{i \in \mathcal{G}} h(p_i^g) \\
(2.4b) \quad & \text{s.t. } c_{ij}^2 + s_{ij}^2 \leq c_{ii}c_{jj} & (i, j) \in \mathcal{L} \\
& (2.2g), (2.3b)-(2.3f) \text{ and } (2.1h)-(2.1j).
\end{aligned}$$

This formulation is useful to reduce the computational complexity and produce a globally optimal solution. In Chapters 3 and 4, we will construct SOCP relaxations of the reactive optimal power flow and multi-period optimal power flow problems on the basis of (2.4).

### 3. REACTIVE OPTIMAL POWER FLOW PROBLEM

#### 3.1 Literature Review

The reactive optimal power flow (ROPF) problem is a variant of the well-known OPF problem in which additional discrete decisions, such as shunt susceptance and tap ratio, are considered. Due to the presence of these discrete variables in the ROPF problem, it can be formulated as a mixed-integer nonlinear programming (MINLP) problem. This chapter utilizes the recent developments in the OPF problem to propose an efficient way of solving the ROPF problem.

OPF is one of the most studied problems in the area of power systems and a variety of solution approaches have been proposed in the literature. Local methods such as the interior point method try to solve the OPF problem but they do not provide any assurances of global optimality. In recent years, convex relaxations of the OPF problem have drawn considerable research interest since the convexity property promises a globally optimal solution under certain conditions. Several approaches have been developed based on convex quadratic (Coffrin et al., 2015b), semidefinite programming (SDP) (Jabr, 2006), second order cone programming (SOCP) (Kocuk et al., 2016) and convex-distflow (Coffrin, Hijazi & Van Hentenryck, 2015a) formulations. The ROPF problem has a similar structure with the OPF problem, except the inclusion of shunt susceptance and tap ratio variables, which are typically modelled as discrete variables. The resulting MINLP problem is difficult to solve and the literature has primarily focused on various heuristic methods (Bakirtzis, Biskas, Zoumas & Petridis, 2002; Capitanescu & Wehenkel, 2010; Nakawiro, Erlich & Rueda, 2011; Sulaiman, Mustafa, Mohamed & Aliman, 2015). The systematic treatment of the ROPF problem is limited to an SDP-based relaxation called *tight-and-cheap relaxation* (TCR) proposed in Bingane, Anjos & Le Digabel (2019).

The contributions of this study are as follows. We propose a completely new MINLP formulation for the ROPF problem along with its mixed-integer second-order cone programming (MISOCP) relaxation. In addition, we improve convex envelopes from the literature and use cutting planes to strengthen the MISOCP relaxation. We also test the accuracy and efficiency of our approach with the TCR method from the literature on difficult test cases and obtain promising results.

### 3.2 Formulations

Consider a power network  $\mathcal{N} = (\mathcal{B}, \mathcal{L})$ , where  $\mathcal{B}$  and  $\mathcal{L}$  denote the set of buses and the set of transmission lines respectively. Let  $\mathcal{G} \subseteq \mathcal{B}$ ,  $\mathcal{S} \subseteq \mathcal{B}$  and  $\mathcal{T}^R \subseteq \mathcal{L}$  respectively denote the set of generators connected to the grid, the buses with a variable shunt susceptance and the lines with a variable tap ratio. Let  $G$  and  $B$  be the matrices of line conductance and susceptance.

The ROPF problem can be modeled as the following MINLP:

$$\begin{aligned}
(3.1a) \quad & \min \sum_{i \in \mathcal{G}} h(p_i^g) \\
(3.1b) \quad & \text{s.t. } p_i^g - p_i^d = g_{ii}|V_i|^2 + \sum_{j \in \delta(i)} p_{ij} \quad i \in \mathcal{B} \\
(3.1c) \quad & q_i^g - q_i^d = -b_{ii}|V_i|^2 + \sum_{j \in \delta(i)} q_{ij} \quad i \in \mathcal{B} \\
(3.1d) \quad & p_{ij} = G_{ij}(|V_i|/\tau_{ij})^2 + (|V_i|/\tau_{ij})|V_j|[G_{ij} \cos(\theta_i - \theta_j) \\
& \quad \quad \quad - B_{ij} \sin(\theta_i - \theta_j)] \quad (i, j) \in \mathcal{L} \\
& p_{ji} = G_{ji}|V_i|^2 + (|V_i|/\tau_{ij})|V_j|[G_{ji} \cos(\theta_i - \theta_j) \\
& \quad \quad \quad - B_{ij} \sin(\theta_i - \theta_j)] \quad (i, j) \in \mathcal{L} \\
(3.1e) \quad & q_{ij} = -B_{ij}(|V_i|/\tau_{ij})^2 - (|V_i|/\tau_{ij})|V_j|[B_{ij} \cos(\theta_i - \theta_j) \\
& \quad \quad \quad + G_{ij} \sin(\theta_i - \theta_j)] \quad (i, j) \in \mathcal{L} \\
& q_{ji} = -B_{ji}|V_i|^2 - (|V_i|/\tau_{ij})|V_j|[B_{ji} \cos(\theta_i - \theta_j) \\
& \quad \quad \quad + G_{ji} \sin(\theta_i - \theta_j)] \quad (i, j) \in \mathcal{L} \\
(3.1f) \quad & \underline{V}_i \leq |V_i| \leq \bar{V}_i \quad i \in \mathcal{B} \\
(3.1g) \quad & \sum_{k \in \mathcal{S}_i} b_{ii}^k \alpha_i^k = b_{ii} \quad i \in \mathcal{B}
\end{aligned}$$

$$\begin{aligned}
(3.1h) \quad & b_{ii} = 0 && i \in \mathcal{B} \setminus \mathcal{S} \\
(3.1i) \quad & \sum_{k \in \mathcal{S}_i} \alpha_i^k = 1, \quad \alpha_i^k \in \{0, 1\} && i \in \mathcal{B} \\
(3.1j) \quad & \sum_{l \in \mathcal{T}_{ij}^R} \frac{\beta_{ij}^l}{\tau_{ij}^l} = 1/\tau_{ij} && (i, j) \in \mathcal{L} \\
(3.1k) \quad & \tau_{ij} = 1 && (i, j) \in \mathcal{L} \setminus \mathcal{T}^R \\
(3.1l) \quad & \sum_{l \in \mathcal{T}_{ij}^R} \beta_{ij}^l = 1, \quad \beta_{ij}^l \in \{0, 1\} && (i, j) \in \mathcal{L} \\
(3.1m) \quad & \underline{q}_i \leq q_i^g \leq \bar{q}_i && i \in \mathcal{G} \\
(3.1n) \quad & \underline{p}_i \leq p_i^g \leq \bar{p}_i && i \in \mathcal{G} \\
(3.1o) \quad & p_{ij}^2 + q_{ij}^2 \leq \bar{S}_{ij}^2, \quad p_{ji}^2 + q_{ji}^2 \leq \bar{S}_{ij}^2 && (i, j) \in \mathcal{L} \\
(3.1p) \quad & |\theta_i - \theta_j| \leq \bar{\theta}_{ij} && (i, j) \in \mathcal{L}.
\end{aligned}$$

Here, the objective function (3.1a) minimizes the total real power generation cost subject to the following constraints: real and reactive power flow balance at bus  $i$  (3.1b)–(3.1c), real and reactive power flow from  $i$  to  $j$  (3.1d)–(3.1e), voltage magnitude bounds at bus  $i$  (3.1f), shunt susceptance selection for bus  $i$  (3.1g), tap ratio selection for line  $(i, j)$  (3.1j), binary restrictions (3.1i)–(3.1l), reactive and real power output of generator  $i$  (3.1m)–(3.1n), apparent flow limit for each line  $(i, j)$  (3.1o) and phase angle limit for each line  $(i, j)$  (3.1p).

### 3.2.1 Alternative

In this section, we propose an alternative MINLP formulation of the ROPF problem motivated by (Kocuk et al., 2016). Let us define a set of new decision variables  $c_{ii}$ ,  $c_{ij}$  and  $s_{ij}$ , respectively representing the quantities  $|V_i|^2$ ,  $|V_i||V_j|\cos(\theta_i - \theta_j)$  and  $s_{ij} := -|V_i||V_j|\sin(\theta_i - \theta_j)$  for  $i \in \mathcal{B}$  and  $(i, j) \in \mathcal{L}$ . More variables are defined as needed below.

We denote the lower (upper) bounds of variables  $c_{ii}, c_{ij}, s_{ij}$  as  $\underline{c}_{ii}, \underline{c}_{ij}, \underline{s}_{ij}$  ( $\bar{c}_{ii}, \bar{c}_{ij}, \bar{s}_{ij}$ ) and set them as follows:

$$\begin{aligned}
\underline{c}_{ii} &:= \underline{V}_i^2, \quad \bar{c}_{ii} := \bar{V}_i^2 && i \in \mathcal{B} \\
\underline{c}_{ij} &:= \bar{V}_i \bar{V}_j \cos(\bar{\theta}_{ij}), \quad \bar{c}_{ij} := \bar{V}_i \bar{V}_j && (i, j) \in \mathcal{L} \\
\underline{s}_{ij} &:= -\bar{V}_i \bar{V}_j \sin(\bar{\theta}_{ij}), \quad \bar{s}_{ij} := \bar{V}_i \bar{V}_j \sin(\bar{\theta}_{ij}) && (i, j) \in \mathcal{L}.
\end{aligned}$$

We will now discuss the constraints in the alternative formulation and their relations with the MINLP in Section 3.2. The updated version of the real power flow balance constraint (3.1b) is given as:

$$(3.2) \quad p_i^g - p_i^d = g_{ii}c_{ii} + \sum_{j \in \delta(i)} p_{ij} \quad i \in \mathcal{B}.$$

Since the variable  $b_{ii}$  can be eliminated from the formulation by substituting  $\sum_{k \in \mathcal{S}_i} b_{ii}^k \alpha_i^k$ , the reactive power flow equation (3.1c) is first rewritten as follows:

$$(3.3) \quad q_i^g - q_i^d = - \left( \sum_{k \in \mathcal{S}_i} b_{ii}^k \alpha_i^k \right) c_{ii} + \sum_{j \in \delta(i)} q_{ij} \quad i \in \mathcal{B}.$$

Then, we define a new variable  $\Gamma_i^k := c_{ii} \alpha_i^k$  to reformulate (3.3) and include additional constraints as follows:

$$(3.4) \quad \begin{aligned} q_i^g - q_i^d &= - \sum_{k \in \mathcal{S}_i} b_{ii}^k \Gamma_i^k + \sum_{j \in \delta(i)} q_{ij} & i \in \mathcal{B} \\ \underline{c}_{ii} \alpha_i^k &\leq \Gamma_i^k \leq \bar{c}_{ii} \alpha_i^k, & i \in \mathcal{B} \\ c_{ii} &= \sum_{k \in \mathcal{S}_i} \Gamma_i^k & i \in \mathcal{B}. \end{aligned}$$

We now update power flow constraints using a similar procedure. In particular, we substitute  $1/\tau_{ij}$  with  $\sum_{l \in \mathcal{T}_{ij}^R} \beta_{ij}^l / \tau_{ij}^l$  into constraints (3.1d) and (3.1e) as follows:

$$(3.5) \quad \begin{aligned} p_{ij} &= G_{ij} \left( |V_i| \sum_{l \in \mathcal{T}_{ij}^R} \frac{\beta_{ij}^l}{\tau_{ij}^l} \right)^2 + \left( |V_i| \sum_{l \in \mathcal{T}_{ij}^R} \frac{\beta_{ij}^l}{\tau_{ij}^l} \right) |V_j| [G_{ij} \cos(\theta_i - \theta_j) - B_{ij} \sin(\theta_i - \theta_j)] \quad (i, j) \in \mathcal{L} \\ q_{ij} &= -B_{ij} \left( |V_i| \sum_{l \in \mathcal{T}_{ij}^R} \frac{\beta_{ij}^l}{\tau_{ij}^l} \right)^2 - \left( |V_i| \sum_{l \in \mathcal{T}_{ij}^R} \frac{\beta_{ij}^l}{\tau_{ij}^l} \right) |V_j| [B_{ij} \cos(\theta_i - \theta_j) + G_{ij} \sin(\theta_i - \theta_j)] \quad (i, j) \in \mathcal{L}. \end{aligned}$$

After defining the new variables  $\bar{\Phi}_{ij}^l := c_{ii} \beta_{ij}^l$ ,  $\Phi_{ij}^l := c_{ij} \beta_{ij}^l$  and  $\Psi_{ij}^l := s_{ij} \beta_{ij}^l$ , we rewrite constraint (3.5) together with the other equations necessary for the lin-

earization as follows:

$$\begin{aligned}
p_{ij} &= \sum_{l \in \mathcal{T}_{ij}^R} \left( G_{ij} \left( \frac{\bar{\Phi}_{ij}^l}{(\tau_{ij}^l)^2} + \frac{\Phi_{ij}^l}{\tau_{ij}^l} \right) - B_{ij} \frac{\Psi_{ij}^l}{\tau_{ij}^l} \right) & (i, j) \in \mathcal{L} \\
p_{ji} &= G_{ji} c_{jj} + \sum_{l \in \mathcal{T}_{ij}^R} \left( G_{ji} \frac{\Phi_{ij}^l}{\tau_{ij}^l} - B_{ji} \frac{\Psi_{ij}^l}{\tau_{ij}^l} \right) & (i, j) \in \mathcal{L} \\
q_{ij} &= - \sum_{l \in \mathcal{T}_{ij}^R} \left( B_{ij} \left( \frac{\bar{\Phi}_{ij}^l}{(\tau_{ij}^l)^2} + \frac{\Phi_{ij}^l}{\tau_{ij}^l} \right) + G_{ij} \frac{\Psi_{ij}^l}{\tau_{ij}^l} \right) & (i, j) \in \mathcal{L} \\
q_{ji} &= -B_{ji} c_{jj} - \sum_{l \in \mathcal{T}_{ij}^R} \left( B_{ji} \frac{\Phi_{ij}^l}{\tau_{ij}^l} + G_{ji} \frac{\Psi_{ij}^l}{\tau_{ij}^l} \right) & (i, j) \in \mathcal{L} \\
\underline{c}_{ii} \beta_{ij}^l &\leq \bar{\Phi}_{ij}^l \leq \bar{c}_{ii} \beta_{ij}^l & l \in \mathcal{T}_{ij}^R, \quad c_{ii} = \sum_{l \in \mathcal{T}_{i,j}^R} \bar{\Phi}_{ij}^l & (i, j) \in \mathcal{L} \\
\underline{c}_{ij} \beta_{ij}^l &\leq \Phi_{ij}^l \leq \bar{c}_{ij} \beta_{ij}^l & l \in \mathcal{T}_{ij}^R, \quad c_{ij} = \sum_{l \in \mathcal{T}_{i,j}^R} \Phi_{ij}^l & (i, j) \in \mathcal{L} \\
\underline{s}_{ij} \beta_{ij}^l &\leq \Psi_{ij}^l \leq \bar{s}_{ij} \beta_{ij}^l & l \in \mathcal{T}_{ij}^R, \quad s_{ij} = \sum_{l \in \mathcal{T}_{i,j}^R} \Psi_{ij}^l & (i, j) \in \mathcal{L}.
\end{aligned} \tag{3.6}$$

We also update the constraint on voltage magnitude bounds (3.1f) as follows:

$$\underline{V}_i^2 \leq c_{ii} \leq \bar{V}_i^2 \quad i \in \mathcal{B}. \tag{3.7}$$

Finally, we define the following consistency constraints for each line  $(i, j)$ :

$$c_{ij}^2 + s_{ij}^2 = c_{ii} c_{jj} \quad (i, j) \in \mathcal{L} \tag{3.8a}$$

$$(\Phi_{ij}^l)^2 + (\Psi_{ij}^l)^2 = \bar{\Phi}_{ij}^l c_{jj} \quad (i, j) \in \mathcal{L}, l \in \mathcal{T}_{ij}^R \tag{3.8b}$$

$$\theta_j - \theta_i = \arctan(s_{ij}/c_{ij}) \quad (i, j) \in \mathcal{L}. \tag{3.8c}$$

Equation (3.8a) preserves the trigonometric relation between the variables  $c_{ii}, c_{ij}$  and  $s_{ij}$ . If we multiply (3.8a) by  $\beta_{ij}^l$ , we can get a similar condition for the variables  $\bar{\Phi}_{ij}^l, \Phi_{ij}^l$  and  $\Psi_{ij}^l$ .

The alternative formulation minimizes (3.1a) subject to constraints (3.1h)–(3.1i), (3.1k)–(3.2) and (3.4)–(3.8c).



### 3.2.2 MISOCP Relaxation

The feasible region of the alternative MINLP formulation is non-convex due to constraints (3.8a)–(3.8c). Let us relax these constraints as follows:

$$(3.9) \quad \begin{aligned} c_{ij}^2 + s_{ij}^2 &\leq c_{ii}c_{jj} & (i, j) \in \mathcal{L} \\ (\Phi_{ij}^l)^2 + (\Psi_{ij}^l)^2 &\leq \bar{\Phi}_{ij}^l c_{jj} & (i, j) \in \mathcal{L}. \end{aligned}$$

Then, an MISOCP relaxation is obtained as (3.1a), (3.1h)–(3.1i), (3.1k)–(3.2), (3.4)–(3.7) and (3.9).

### 3.2.3 Tightened MISOCP Relaxation

To tighten the MISOCP relaxation, we also consider an outer-approximation of constraints (3.8a) and (3.8c), which is an improved version of a similar approach proposed in Kocuk et al. (2018). Let us define the set  $\mathcal{P} = [\underline{c}, \bar{c}] \times [\underline{s}, \bar{s}] \times [\underline{\theta}, \bar{\theta}]$  and consider

$$\mathcal{A} := \left\{ (c, s, \theta) \in \mathcal{P} : \theta = \arctan(s/c), \underline{c}^2 \leq c^2 + s^2 \leq \bar{c}^2 \right\},$$

where  $\theta_i - \theta_j$  is denoted by  $\theta$  and the other subscripts are omitted. The four points of interest are given as follows:

$$\begin{aligned} \zeta^1 &= (\underline{c}, \bar{s}, \arctan(\bar{s}/\underline{c})), & \zeta^2 &= (\bar{c}, \bar{s}, \arctan(\bar{s}/\bar{c})), \\ \zeta^3 &= (\bar{c}, \underline{s}, \arctan(\underline{s}/\bar{c})), & \zeta^4 &= (\underline{c}, \underline{s}, \arctan(\underline{s}/\underline{c})). \end{aligned}$$

The following proposition provides two upper envelopes for  $\mathcal{A}$ :

**Proposition 1** *Let  $\theta = \gamma^1 + \mu^1 c + v^1 s$  and  $\theta = \gamma^2 + \mu^2 c + v^2 s$  be the planes passing through points  $\{\zeta^1, \zeta^2, \zeta^3\}$ , and  $\{\zeta^1, \zeta^3, \zeta^4\}$ , respectively. Then, two valid inequalities for  $\mathcal{A}$  can be obtained as*

$$\bar{\gamma}^m + \mu^m c + v^m s \geq \arctan(s/c),$$

with  $\bar{\gamma}^m = \gamma^m + \Delta^m$ ,  $m = 1, 2$ , where

$$(3.10) \quad \Delta^m = \max_{(c,s,\theta) \in \mathcal{A}} \{ \arctan(s/c) - (\gamma^m + \mu^m c + v^m s) \}.$$

We will omit the proof of Proposition 1 since the statement holds true by construction. However, the interesting property related to the optimization problem (3.10) is that although both its objective function and feasible region are nonconvex, it can still be solved globally. The key idea is to re-state this optimization problem in the polar coordinates as

$$(3.11) \quad \Delta^m = -\gamma^m + \max_{r \in [\underline{c}, \bar{c}], \theta \in [\underline{\theta}, \bar{\theta}]} \{\theta - r(\mu^m \cos(\theta) + v^m \sin(\theta))\},$$

where  $r := \sqrt{c^2 + s^2}$ . Since problem (3.11) is linear in  $r$ , it can be solved for the two end-points of the interval  $[\underline{c}, \bar{c}]$  separately. Finally, the remaining one-dimensional optimization problems in  $\theta$  can be solved by checking the KKT points. We note that Proposition 1 is an improvement over Proposition 3.8 from Kocuk et al. (2018) since the feasible region of problem (3.10) is a smaller subset of the corresponding optimization problem in Kocuk et al. (2018).

We also obtain two under envelopes for  $\mathcal{A}$ .

**Proposition 2** *Let  $\theta = \gamma^3 + \mu^3 c + v^3 s$  and  $\theta = \gamma^4 + \mu^4 c + v^4 s$  be the planes passing through points  $\{\zeta^1, \zeta^2, \zeta^4\}$ , and  $\{\zeta^2, \zeta^3, \zeta^4\}$ , respectively. Then, two valid inequalities for  $\mathcal{A}$  are defined as*

$$\bar{\gamma}^n + \mu^n c + v^n s \leq \arctan(s/c)$$

with  $\bar{\gamma}^n = \gamma^n - \Delta^n$ ,  $n = 3, 4$ , where

$$\Delta^n = \max_{(c, s, \theta) \in \mathcal{A}} \{(\gamma^n + \mu^n c + v^n s) - \arctan(s/c)\}.$$

Finally, we add the following valid inequalities to the MISOCP relaxation:

$$\begin{aligned} \bar{\gamma}_{ij}^m + \mu_{ij}^m c_{ij} + v_{ij}^m s_{ij} &\geq \theta_j - \theta_i \quad m = 1, 2, (i, j) \in \mathcal{L} \\ \bar{\gamma}_{ij}^n + \mu_{ij}^n c_{ij} + v_{ij}^n s_{ij} &\leq \theta_j - \theta_i \quad n = 3, 4, (i, j) \in \mathcal{L}. \end{aligned}$$

We will use the abbreviation MISOCPA to refer to this stronger relaxation.

Additionally, we generate cutting planes for each cycle in the cycle basis using a method called *SDP Separation*; more details can be found in Kocuk et al. (2016). We denote this further improved relaxation as MISOCPA+.

### 3.3 Solution Approach

We first solve the continuous relaxation of the MISOCPA formulation by relaxing the integrality of  $\alpha_i^k$  and  $\beta_{ij}^l$  variables. Then, for each cycle in the cycle basis, we use the SDP separation method to generate cutting planes to separate this continuous relaxation solution from the feasible region of the SDP relaxation of the cycle. The separation process is parallelized over cycles. We repeat this procedure five times consecutively. Then, we solve the final MISOCPA+ relaxation to obtain a lower (LB) bound, and then fix the binary variables in the MINLP formulation to obtain an upper bound (UB) from the remaining nonlinear program (NLP) using a local solver, which provides a feasible solution to the ROPF problem. The optimality gap is computed as  $\%Gap = 100 \times (1 - LB/UB)$ .

### 3.4 Computational Experiments

We compare the percentage optimality gap and the computational time of the MISOCPA+ approach with the publicly available implementation of TCR relaxation of Type 2 (TCR2) from Bingane et al. (2019) under default settings. All computational experiments have been carried out on a 64-bit desktop with Intel Core i7 CPU with 3.20GHz processor and 64 GB RAM. Our code is written in Python language using Spyder environment. The solvers Gurobi, IPOPT and MOSEK are used to solve the MISOCPA+ relaxation, NLP and separation problems, respectively. We run Gurobi with the default settings except for changing the time limit as 30 seconds.

For the computational experiments, we use the OPF instances from the NESTA library; typical operating conditions, congested operating conditions (API) and small angle difference conditions (SAD). We only consider difficult instances in which the SOCP optimality gap is more than 1% Kocuk et al. (2016).

The sets of the discrete values are determined as  $b_{ii}^k \in \{0, 1\}$  for  $i \in \mathcal{S}$  and  $\tau_{ij}^l \in \{1 \pm 0.0125 \times h : h \in \{0, 1, \dots, 8\}\}$  for  $(i, j) \in \mathcal{T}^R$ , which represent the on/off status of the shunt susceptance and values of the tap ratio, respectively.

Table 3.1 Computational results with 0.0125 discretization step size. Instances with the SOCP optimality gap above 3% are indicated with an asterisk.

Case	TCR2				MISOCPA+			
	LB	Time	UB	%Gap	LB	Time	UB	%Gap
3lmbd	5769.87	0.65	5812.64	0.74	5780.75	0.59	5812.64	0.55
5pjm*	15313.38	0.72	17551.89	12.75	16504.27	0.23	17551.89	5.97
30ieee*	205.19	1.13	205.24	0.02	205.13	4.59	205.24	0.05
118ieee	3695.39	4.66	3714.77	0.52	3685.97	34.45	3717.48	0.85
<b>Average</b>		<b>1.79</b>		<b>3.51</b>		<b>9.97</b>		<b>1.86</b>
3lmbd_api*	363.00	0.66	367.74	1.29	362.89	0.11	367.74	1.32
6ww_api*	273.76	0.53	273.76	0.00	273.64	0.37	273.76	0.04
14ieee_api	319.12	0.93	319.87	0.23	318.87	1.34	320.92	0.64
30as_api*	559.96	2.38	571.13	1.96	562.25	0.92	571.13	1.55
30fsr_api*	213.93	2.16	372.14	42.51	227.69	0.89	372.11	38.81
39epri_api	7333.40	2.59	7495.37	2.16	7208.84	31.33	7473.25	3.54
118ieee_api*	5932.26	4.47	10171.50	41.68	5923.71	34.47	10185.71	41.84
<b>Average</b>		<b>1.96</b>		<b>12.83</b>		<b>9.92</b>		<b>12.53</b>
3lmbd_sad*	5831.07	0.57	5992.72	2.70	5869.13	0.12	5992.72	2.06
4gs_sad*	321.55	0.58	324.02	0.76	323.65	0.13	324.02	0.12
5pjm_sad*	25560.36	0.62	26423.33	3.27	26419.24	0.18	26423.32	0.02
9wscc_sad	5521.49	0.54	5590.09	1.23	5589.55	0.2	5590.09	0.01
29edin_sad*	31173.80	3.19	46933.31	33.58	36290.42	3.78	45883.89	20.91
30as_sad*	903.09	2.32	914.44	1.24	906.93	1.12	914.44	0.82
30ieee_sad*	205.30	0.96	205.35	0.02	205.21	4.25	205.34	0.06
118ieee_sad*	3869.62	4.66	4281.41	9.62	3984.37	34.46	4296.00	7.25
<b>Average</b>		<b>1.68</b>		<b>6.55</b>		<b>5.53</b>		<b>3.91</b>
<b>Overall Average</b>		<b>1.81</b>		<b>8.23</b>		<b>8.08</b>		<b>6.65</b>
<b>Overall Average*</b>		<b>1.78</b>		<b>10.81</b>		<b>6.12</b>		<b>8.63</b>

Table 3.2 Computational results with 0.05 discretization step size. Instances with the SOCP optimality gap above 3% are indicated with an asterisk.

Case	TCR2				MISOCPA+			
	LB	Time	UB	%Gap	LB	Time	UB	%Gap
3lmbd	5769.87	0.65	5812.64	0.74	5780.75	0.56	5812.64	0.55
5pjm*	15313.38	0.72	17551.89	12.75	16504.27	0.23	17551.89	5.97
30ieee*	205.2	1.13	205.25	0.02	205.15	1.42	205.25	0.05
118ieee	3695.39	4.66	3714.67	0.52	3688.39	15.41	3714.41	0.7
<b>Average</b>		<b>1.79</b>		<b>3.51</b>		<b>4.41</b>		<b>1.82</b>
3lmbd_api*	362.99	0.66	367.74	1.29	362.89	0.12	367.74	1.32
6ww_api*	273.76	0.53	273.76	0	273.64	0.36	273.76	0.04
14ieee_api	319.12	0.93	320.16	0.32	318.87	0.71	321.22	0.73
30as_api*	559.96	2.38	571.13	1.96	562.25	0.93	571.13	1.55
30fsr_api*	213.93	2.16	372.14	42.51	227.69	0.92	372.11	38.81
39epri_api	7333.4	2.59	7481.14	1.97	7263.86	13.31	7474.46	2.82
118ieee_api*	5932.26	4.47	10143.75	41.52	5951.21	23.69	10198.57	41.65
<b>Average</b>		<b>1.96</b>		<b>12.80</b>		<b>5.72</b>		<b>12.42</b>
3lmbd_sad*	5831.07	0.57	5992.72	2.70	5869.13	0.13	5992.72	2.06
4gs_sad*	321.55	0.58	324.02	0.76	323.65	0.13	324.02	0.12
5pjm_sad*	25560.36	0.62	26423.33	3.27	26419.24	0.18	26423.32	0.02
9wscc_sad	5521.49	0.54	5590.09	1.23	5589.55	0.2	5590.09	0.01
29edin_sad*	31173.8	3.19	46933.31	33.58	36307.34	3.35	45886.11	20.88
30as_sad*	903.09	2.32	914.44	1.24	906.93	1.1	914.44	0.82
30ieee_sad*	205.3	0.96	205.37	0.03	205.26	1.41	205.37	0.06
118ieee_sad*	3869.62	4.66	4303.63	10.08	4004.72	8.79	4293.96	6.74
<b>Average</b>		<b>1.68</b>		<b>6.61</b>		<b>1.91</b>		<b>3.84</b>
<b>Overall Average</b>		<b>1.81</b>		<b>8.24</b>		<b>3.84</b>		<b>6.57</b>
<b>Overall Average*</b>		<b>1.78</b>		<b>10.84</b>		<b>3.05</b>		<b>8.58</b>

The results of our computational experiments are reported in Table 3.1. The computational time is measured in seconds and includes the time spent for solving the separation problems. If we compare the averages of optimality gap, MISOCPA+ outperforms TCR2 in all types of NESTA instances. MISOCPA+ has the best performance on SAD instances and dominates TCR2 in all of them. Overall, we note that MISOCPA+ relaxation has more accurate solutions with 6.65% optimality gap, on average, than TCR with 8.23%. In terms of computational time, MISOCPA+ is slower with 8.08 seconds, on average, than TCR2 with 1.81. We also point out the even better performance MISOCPA+ in terms of accuracy on more difficult instances with the SOCP gap more than 3%.

### 3.4.1 The Effect of Tap Ratio Discretization

We also analyze the effect of tap ratio discretization on the ROPF problem. The algorithm is repeated with a different discrete set  $\tau_{ij}^l \in \{1 \pm 0.05 \times h : h \in \{0, 1, 2\}\}$  for  $(i, j) \in \mathcal{T}^R$ . The results are reported in Table 3.2. We observe that UBs and optimality gaps do not change significantly with this coarser discretization. In fact, the average absolute percentage change of UBs is only 0.02%. Since the computational effort increases with the number of discrete steps, we conclude it may be more practical to use a small number of discrete steps, especially for small size test cases.

### 3.4.2 A Test Case for a Larger Instance

In order to solve a large scale instance within acceptable time limits, we modify our algorithm as follows: The final MISOCPA+ relaxation is also solved by relaxing the integrality of  $\alpha_i^k$  and  $\beta_{ij}^l$  variables. The convex combinations of discrete values  $\{b_{ii}^k : k \in \mathcal{S}_i\}$  and  $\{\tau_{ij}^l : l \in \mathcal{T}_{ij}^R\}$  with coefficients  $\alpha_i^k$  and  $\beta_{ij}^l$  are rounded off to the nearest discrete value in these sets. Then, we fix the binary variables with respect to the rounded-off values in the MINLP formulation. Once tested on 1354-bus PEGASE SAD test case, the modified algorithm produces a feasible solution with a cost of \$1,220,718 with an optimality gap of 3.82% in approximately 6 minutes. We note that the TCR2 relaxation experiences numerical difficulties for this test case.

### 3.5 Conclusions

In this chapter, we propose an MISOCP-based approach, namely MISOCPA+, to approximate globally optimal solutions of the ROPF problem. The accuracy and efficiency of this approach are compared with TCR2 using difficult OPF instances from the NESTA library. The computational results indicate that MISOCPA+ is quite promising to solve any type of instances accurately, especially the ones with small angle conditions.

## 4. MULTI-PERIOD OPTIMAL POWER FLOW PROBLEM WITH ELECTRIC VEHICLES

### 4.1 Introduction

With the advent of electric vehicles (EV), the OPF studies that consider large scale integration of EVs have become increasingly important. While the classical OPF problem only considers a single period planning, the interconnection of the energy storage of EVs with the power network makes it necessary to solve multi-period OPF. The MOPF problem optimizes operations of the power grid with respect to a certain objective and network constraints over a finite planning horizon. Large scale integration of EVs requires additional settings and limitations and, therefore, problem complexity and computational effort increase. EV charging creates extra demand on the grid and in the case of Vehicle to Grid (V2G) systems, EVs can also supply power to the grid. This bidirectional flow with its impacts on the grid and several other aspects, such as penetration level, driving profiles, and battery characteristics, need to be taken into consideration in the model formulation.

Integrating EV charging stations to power systems changes the dynamics of conventional power distribution and poses considerable challenges to network operations under an uncoordinated charging scenario. For example, flexible EV charging patterns might increase the peak load of the power grid and cause overload on transmission lines; consequently, this increases power generation cost and damages power system security. Coordinated charging is critical for overcoming the security and economy issues of the grid operations. On the other hand, with the coordinated charging strategies, one can turn the flexibility of EVs into an advantage by flattening peak load and filling load valleys.

EVs create a considerable opportunity for reduction of greenhouse gas emissions



from transportation compared to conventional vehicles. However, the additional electricity generation to charge EVs may cause greenhouse gas emissions depending on the source of electricity generation (Yuksel, Tamayao, Hendrickson, Azevedo & Michalek, 2016). For example, coal-based generation results in significant amounts of emissions into the atmosphere. Therefore, it is also critical to consider additional emissions generated by power plants to exploit EVs' environmental benefits.

Many countries such as the United States government set targets to render EVs competitive with fossil fuel vehicles. Many federal and local tax credits and other incentives are granted to promote the use of EV (AFDC, 2017). In the future, EVs' charging demand can comprise a major part of the electricity consumption. With the large scale deployment of EVs, charging strategies will become more critical from different perspectives such as network operators, financial parties, EV drivers, and environmental policy.

#### **4.1.1 Literature Review**

The incorporation of a large number of EVs into power systems can cause various complications in operations under uncoordinated charging scenario. These complications include increased network losses, overloaded transmission lines, unbalanced voltage and increased peak load, resulting in a significant increase in electricity generation cost and damage to power system security. To address these issues, various coordinated charging strategies of EVs have been developed in recent years. Clement-Nyns, Haesen & Driesen (2009) show that power losses and voltage deviations can be reduced by flattening load profile if the charging of EVs is coordinated. In order to fill the load valley, Gan, Topcu & Low (2012) schedule EV charging using a decentralized algorithm. Masoum, Moses & Hajforoosh (2012) investigate the effects of coordinated charging on transformer loading and use a real-time algorithm to minimize the stress on transformers. However, they note that the proposed approach may not be satisfactory in the case where the penetration level of EV is very high.

Vehicle-to-Grid (V2G) emerged as a promising concept with the goal to compensate the power mismatch between generation and load. This concept was firstly presented in Kempton & Letendre (1997), and its economic feasibility and adaptability are studied in Kempton & Tomić (2005) and Tomić & Kempton (2007). The subsequent studies such as Andersson, Elofsson, Galus, Göransson, Karlsson, Johnsson & Andersson (2010); Saber & Venayagamoorthy (2010); Sortomme & El-Sharkawi

(2010) integrate V2G technology into the distribution network to exploit its economic and environmental benefits. Additional benefits of V2G, such as regulation of real power, load balancing, peak load shaving, valley filling and reactive power support, are discussed in Yilmaz & Krein (2012). The aggregator, which controls a fleet of the EVs to function as a source of generation, is a key concept for implementing V2G technology (Guille & Gross, 2009). In Ortega-Vazquez, Bouffard & Silva (2012) and Schuller, Dietz, Flath & Weinhardt (2014), the aggregation for EV charging strategies is further analyzed in V2G context.

In the past decades, several heuristic solution approaches have been developed to coordinate the charging of EVs. Hutson, Venayagamoorthy & Corzine (2008) present a binary particle swarm optimization to maximize EV users' profit under the network and EV charging constraints. A simulated annealing based optimization is employed in the plug-in EV (PEV) charging problem to minimize total system cost in Valentine, Temple & Zhang (2011). Alonso, Amaris, Germain & Galan (2014) propose a genetic algorithm optimization approach to flatten the load profile while taking into consideration PEV users' behavior and network technical limits, including apparent flow limit and voltage limit. In Yang, Li, Niu, Xue & Foley (2014), a self-learning teaching-learning based optimization variant is introduced to solve a dynamic economic dispatch problem integrating different PEV charging scenarios. A more comprehensive list of these heuristic approaches can be found in Yang, Li & Foley (2015).

Convex relaxations of the single-period OPF problem have been widely studied (refer to Chapter 2), however very few studies focus on convex relaxations of MOPF problem. Li, Gan, Chen & Low (2012) model a demand response problem in radial distribution networks as an AC OPF problem ignoring reactive power. This optimization problem is convexified and extended to an AC MOPF problem. Gopalakrishnan, Raghunathan, Nikovski & Biegler (2013) solve the AC MOPF problem using an SDP relaxation, and Jabr (2014) proposes an SOCP relaxation of the AC MOPF problem for distribution networks with photovoltaics. The paper by Huang, Wu, Wang & Zhao (2016) formulates the AC MOPF with the planning of EV charging as an SOCP problem in which generator limits are ignored.

Several studies focus on the OPF problem that considers the integration of EVs in recent years. Judd & Overbye (2008) solve the OPF and the security-constrained OPF problems for a single period. Then, they analyze the effect of EV penetration on cost reduction by solving the problems once more with the inclusion of the EVs as generators. In order to minimize power losses while avoiding the usage of tap changers, Acha, Green & Shah (2010) propose a time coordinated OPF (TCOPF)

model with network and EV charging constraints, however, the effects of EV charging on power system security are not considered. The paper by Acha, Green & Shah (2011) suggest a similar TCOPF model to minimize both energy and emission costs. Yang, He & Fu (2014) present an OPF strategy to schedule charging and discharging of EVs considering EV drivers' satisfaction and the grid cost, and use improved particle swarm optimization algorithm based on genetic variation and simulated annealing. However, the simulation is only performed on a small size system. Zakariazadeh, Jadid & Siano (2014) formulate a multi-objective optimization problem in order to minimize both operational costs and emission. They decompose an MINLP model into an MILP master problem consisting of EV charging constraints and an NLP problem based on the OPF. Fan, Duan, Zhang, Jiang, Mao & Wang (2017) utilize the decomposability of alternating direction method of multipliers to solve the MOPF problem and divide the problem into two subproblems: first, to dispatch charging power to each aggregator; second, to distribute the total power of aggregator to each EV controlled by the aggregator.

There are some missing aspects of EV charging strategies in the literature. In Tang & Zhang (2016), the authors do not consider physical limitations and assume that EVs can be fully charged during a single period. In some of the previous works, power grid security constraints are ignored such as line flow (Fan et al., 2017), generator (Wang, Bharati, Paudyal, Ceylan, Bhattarai & Myers, 2019) and voltage limits. Many existing studies incorporate only a small number of EVs (Chen, Tan & Quek, 2014) or charging stations (Fan et al., 2017). Shi, Tuan, Savkin, Duong & Poor (2018) consider only economic aspects without environmental impacts. Azizipanah-Abarghooee, Terzija, Golestaneh & Roosta (2016) consider both operation cost and emission objectives; however, they do not guarantee to produce globally optimal solutions and carry out comprehensive tests only on small size networks. Several studies, such as (Fan et al., 2017), do not consider the behavior of EV users and randomly generate arrival times.

#### 4.1.2 Contributions

The main contributions of this chapter are summarized as follows:

- We introduce a new MOPF formulation for the joint problem of OPF and EV charging by bringing together test cases and real data for electricity consumption, marginal emission factors, and EV driving profiles.

- We develop a convex optimization framework. Specifically, we introduce an SOCP model in which an emission constraint is imposed to restrict emissions related to EV charging from power plants. EV charging constraints and their effects on the power system are also taken into account.
- We demonstrate the effectiveness of the proposed approach on three test cases with up to 2000 buses from PGLIB-OPF. Our algorithm is able to solve large scale test cases in reasonable computation time and offer guarantees of global optimality with very small optimality gaps.
- Our extensive computational experiments suggest that through coordinated charging of EVs, marginal emission can be decreased while keeping the marginal cost constant, and the integration of the V2G concept leads to cost savings, despite assuming hourly electricity prices are constant.

The remainder of this chapter is organized as follows. Section 4.2 describes the problem, and provides an alternative formulation and its SOCP relaxation. Section 4.3 introduces our approach to solve this optimization problem. Section 4.4 defines the input data used in the formulation. Section 4.5 presents the experimental setup and the computational results.

## 4.2 Formulations

In this section, we present our mathematical programming formulation and its SOCP relaxation. We formulate an MOPF problem that coordinates the charging of EVs. The model minimizes the total cost of generation over a finite planning horizon while determining the optimal schedule of power generation and EV charging. We take into account both network constraints and EV charging constraints. We consider only power station emissions associated with EV charging. Therefore, we utilize marginal emissions, which occur to satisfy the additional demand due to EVs. The EV charging constraints are formulated based on actual EV driving profiles that provide arrival and departure times of each trip and energy requirements for each period. We assume that only real power can be consumed by EV and fed back to the grid. All EVs connected to the same bus are aggregated as an entity. In the formulation, we will use the term EV to refer to a fleet of EV charged at the same bus. Note that our formulation considers aggregate charging load and requires perfect knowledge of the user’s driving behavior and electricity consumption.

Consider a power network  $\mathcal{N} = (\mathcal{B}, \mathcal{L})$ , where  $\mathcal{B}$  denotes the node set, i.e., the set of buses, and  $\mathcal{L}$  denotes the edge set, i.e., the set of transmission lines. Let  $\mathcal{G} \subseteq \mathcal{B}$  denote the set of generators and  $\mathcal{T} = \{1, \dots, T\}$  represents the time periods.  $\mathcal{D} \subseteq \mathcal{B}$  is the set of buses with real power load.

We present the following formulation of the MOPF problem:

$$\begin{aligned}
(4.1a) \quad & \min \sum_{i \in \mathcal{G}} \sum_{t \in \mathcal{T}} (p_{it}^g L_i + (p_{it}^g)^2 Q_i) \\
(4.1b) \quad & \text{s.t. } p_{it}^g - p_{it}^d - a_{it} + \eta_i b_{it} = g_{ii} |V_{it}|^2 + \sum_{j \in \delta(i)} p_{ijt} \quad i \in \mathcal{B}, t \in \mathcal{T} \\
(4.1c) \quad & q_{it}^g - q_{it}^d = -b_{ii} |V_{it}|^2 + \sum_{j \in \delta(i)} q_{ijt} \quad i \in \mathcal{B}, t \in \mathcal{T} \\
(4.1d) \quad & p_{ijt} = G_{ij} |V_{it}|^2 + |V_{it}| |V_{jt}| [G_{ij} \cos(\theta_{it} - \theta_{jt}) \\
& \quad \quad \quad - B_{ij} \sin(\theta_{it} - \theta_{jt})] \quad (i, j) \in \mathcal{L}, t \in \mathcal{T} \\
(4.1e) \quad & q_{ijt} = -B_{ij} |V_{it}|^2 - |V_{it}| |V_{jt}| [B_{ij} \cos(\theta_{it} - \theta_{jt}) \\
& \quad \quad \quad + G_{ij} \sin(\theta_{it} - \theta_{jt})] \quad (i, j) \in \mathcal{L}, t \in \mathcal{T} \\
(4.1f) \quad & \underline{V}_i \leq |V_{it}| \leq \bar{V}_i \quad i \in \mathcal{B}, t \in \mathcal{T} \\
(4.1g) \quad & \underline{p}_i \leq p_{it}^g \leq \bar{p}_i \quad i \in \mathcal{G}, t \in \mathcal{T} \\
(4.1h) \quad & \underline{q}_i \leq q_{it}^g \leq \bar{q}_i \quad i \in \mathcal{G}, t \in \mathcal{T} \\
(4.1i) \quad & p_{ijt}^2 + q_{ijt}^2 \leq \bar{S}_{ij}^2 \quad (i, j) \in \mathcal{L}, t \in \mathcal{T} \\
(4.1j) \quad & |\theta_{it} - \theta_{jt}| \leq \bar{\theta}_{ij} \quad (i, j) \in \mathcal{L}, t \in \mathcal{T} \\
(4.1k) \quad & s_{it} + \eta_i a_{it} - b_{it} - c_{it} = s_{i(t+1)} \quad i \in \mathcal{B}, t \in \{0\} \cup \mathcal{T} \\
(4.1l) \quad & \underline{s}_{it} \leq s_{it} \leq \bar{s}_{it} \quad i \in \mathcal{B}, t \in \mathcal{T} \\
(4.1m) \quad & s_{i0} = I_i \bar{s}_{i0} \quad i \in \mathcal{B} \\
(4.1n) \quad & s_{i(T+1)} \geq I_i \bar{s}_{i(T+1)} \quad i \in \mathcal{B} \\
(4.1o) \quad & 0 \leq a_{it} \leq \bar{a}_{it} \quad i \in \mathcal{B}, t \in \mathcal{T} \\
(4.1p) \quad & 0 \leq b_{it} \leq \bar{b}_{it} \quad i \in \mathcal{B}, t \in \mathcal{T} \\
(4.1q) \quad & \sum_{i \in \mathcal{B}} \sum_{t \in \mathcal{T}} e_{it} a_{it} \leq \bar{E}.
\end{aligned}$$

Here, the objective function (4.1a) aims to minimize the total cost of power generation. Constraint (4.1b) ensures real power flow balance at bus  $i$ , while considering EV charging and discharging power. Constraint (4.1c) ensures reactive power flow balance at bus  $i$ . Constraints (4.1d) and (4.1e) represent the real and reactive power flow, respectively. Constraint (4.1f) enforce bus voltage magnitude to maintain a level under acceptable limitations. Constraints (4.1g) and (4.1h) limit real and reactive power outputs of generator  $i$ . Also, we set  $\underline{p}_i = \bar{p}_i = \underline{q}_i = \bar{q}_i = 0$  for  $i \in \mathcal{B} \setminus \mathcal{G}$ .

Constraint (4.1i) satisfy transmission capacity limitations of line  $(i, j)$ . Constraint (4.1j) sets restrictions on phase angle. Constraint (4.1k) ensures balance between power supply and EV demand. Constraint (4.1l) controls the load of EV battery in a specified range between the minimum charging requirement and the maximum battery capacity in order to satisfy the charging demand of the EV. Constraint (4.1m) and (4.1n) set the battery state of charge at the beginning and end of the planning horizon, respectively. Constraints (4.1o) and (4.1p) limit the charging and discharging rate of EV. If an EV is connected to the grid at time  $t$ , its charging/discharging rate should be between zero and the maximum limit. Otherwise, maximum allowable charging and discharging limits  $(\bar{a}_{it}, \bar{b}_{it})$  are set to zero. Constraint (4.1q) sets an upper on the total amount of emission allowed.

#### 4.2.1 Alternative Formulation

In this section, we present an alternative formulation for the mathematical model (4.1) motivated by the reformulation in Section 2.2.3. Let us first define the new decision variables:

- For each bus  $i \in \mathcal{B}$  and time  $t \in \mathcal{T}$ ,
  - $c_{iit} := |V_{it}|^2$ .
- For each line  $(i, j) \in \mathcal{L}$  and time  $t \in \mathcal{T}$ ,
  - $c_{ijt} := |V_{it}||V_{jt}|\cos(\theta_{ij} - \theta_{jt})$
  - $s_{ijt} := -|V_{it}||V_{jt}|\sin(\theta_{it} - \theta_{jt})$ .

Then, we denote the lower (upper) bounds of variables  $c_{iit}, c_{ijt}, s_{ijt}$  as  $\underline{c}_{ii}, \underline{c}_{ij}, \underline{s}_{ij}$  ( $\bar{c}_{ii}, \bar{c}_{ij}, \bar{s}_{ij}$ ), respectively. We can set these bounds as follows:

- For each bus  $i \in \mathcal{B}$  and time  $t \in \mathcal{T}$ ,
  - $\underline{c}_{ii} := \underline{V}_i^2, \bar{c}_{ii} := \bar{V}_i^2$ .
- For each line  $(i, j) \in \mathcal{L}$  and time  $t \in \mathcal{T}$ ,
  - $\underline{c}_{ij} := \bar{V}_i \bar{V}_j \cos(\bar{\theta}_{ij}), \bar{c}_{ij} := \bar{V}_i \bar{V}_j$ ,
  - $\underline{s}_{ij} := -\bar{V}_i \bar{V}_j \sin(\bar{\theta}_{ij}), \bar{s}_{ij} := \bar{V}_i \bar{V}_j \sin(\bar{\theta}_{ij})$ .

To eliminate the nonlinearities, we rewrite the constraints (4.1b)–(4.1f) replacing

the newly defined variables as follows:

$$(4.2a) \quad p_{it}^g - p_{it}^d - a_{it} + \eta_i b_{it} = g_{ii} c_{iit} + \sum_{j \in \delta(i)} p_{ijt} \quad i \in \mathcal{B}, t \in \mathcal{T}$$

$$(4.2b) \quad q_{it}^g - q_{it}^d = -b_{ii} c_{iit} + \sum_{j \in \delta(i)} q_{ijt} \quad i \in \mathcal{B}, t \in \mathcal{T}$$

$$(4.2c) \quad p_{ijt} = G_{ij} \frac{c_{iit}}{(\tau_{ij})^2} + \frac{[G_{ij} c_{ijt} - B_{ij} s_{ijt}]}{\tau_{ij}} \quad (i, j) \in \mathcal{L}, t \in \mathcal{T}$$

$$(4.2d) \quad q_{ijt} = -B_{ij} \frac{c_{iit}}{(\tau_{ij})^2} - \frac{[B_{ij} c_{ijt} + G_{ij} s_{ijt}]}{\tau_{ij}} \quad (i, j) \in \mathcal{L}, t \in \mathcal{T}$$

$$(4.2e) \quad \underline{V}_i^2 \leq c_{iit} \leq \bar{V}_i^2 \quad i \in \mathcal{B}, t \in \mathcal{T}.$$

We define the following consistency constraints which preserves the trigonometric relation between the variables  $c_{iit}, c_{ijt}$  and  $s_{ijt}$ :

$$(4.3a) \quad c_{ijt}^2 + s_{ijt}^2 = c_{iit} c_{jjt} \quad (i, j) \in \mathcal{L}, t \in \mathcal{T}$$

$$(4.3b) \quad \theta_{jt} - \theta_{it} = \text{atan2}(s_{ijt}, c_{ijt}) \quad i \in \mathcal{B}, t \in \mathcal{T}.$$

The alternative formulation minimizes the objective function (4.1a), under the constraints (4.1g)–(4.1q), (4.2) and (4.3).

#### 4.2.2 SOCP Relaxations

The feasible region of the alternative NLP formulation is nonconvex due to constraints (4.3). We eliminate the constraint (4.3b) and relax the constraint (4.3a) as follows:

$$(4.4) \quad c_{ijt}^2 + s_{ijt}^2 \leq c_{iit} c_{jjt} \quad (i, j) \in \mathcal{L}, t \in \mathcal{T}.$$

Then, an SOCP relaxation of the MOPF problem is obtained as (4.1a), (4.1g)–(4.1q), (4.2) and (4.4).

### 4.3 Solution Approach

In this section, we present our solution approach for the optimization problem (4.1) to find a globally optimal solution. The presented problem is nonlinear and nonconvex, which may cause solvers to produce a locally optimal solution. The purpose of relaxing the problem as an SOCP problem is to find a globally optimal solution; however, a relaxation is not sufficient to guarantee convergence to an optimal solution of the original problem. Therefore we aim to construct lower and upper bounds, which come from the relaxation and the original problem, respectively. If the optimal solution of the relaxation is contained in the feasible region of the original problem, which means the lower bound equals the upper bound, the algorithm provides an optimality guarantee. Otherwise, the lower bound gives a quality measure of the upper bound.

Initially, we start solving the SOCP relaxation from Section 4.2.2 to obtain a lower bound (LB). The next step is to solve the MOPF model (4.1) to obtain an upper bound. Since the problem is challenging to solve, we fix the charging and discharging power variables  $a_{it}$  and  $b_{it}$  to the optimal values obtained from the SOCP relaxation in the MOPF model and eliminate EV charging constraints (4.1k)–(4.1q). Now the remaining problem is separable; we decompose the problem into smaller size subproblems, one for each time. The single period NLP formulation corresponds to model (2.2) where  $p_i^d = p_i^d + a_i - \eta_i b_i$ . We solve this problem for each period and sum up its objective values to obtain an upper bound (UB). The optimality gap is computed as  $\%Gap = 100 \times (1 - LB/UB)$ .

We introduce Algorithm 1 in order to observe the relation between marginal emissions and total generation cost. We first consider cost and emission objectives separately to obtain levels of emission, then perform optimization for the different settings of emission parameter  $\bar{E}$ . This is like a multi-objective approach and the aim is to approximate the Pareto frontier. Solving the SOCP formulation under the emission minimization objective, we first find a lower bound on emission (LBE) while satisfying the operation and security constraints. To find an upper bound on emission (UBE), we solve the problem under the cost minimization objective and calculate the marginal emission. Then, we select  $\bar{E}$  values varying on a logarithmic scale within the LBE and UBE. For the different settings of  $\bar{E}$ , we repeat the optimization algorithm to find the upper and lower bounds of the MOPF problem.



---

**Algorithm 1**

---

- 1:  $\text{LBE} = \min\{\sum_{i \in \mathcal{B}} \sum_{t \in \mathcal{T}} e_{it} a_{it} : (4.1\text{g})\text{--}(4.1\text{q}), (4.2), (4.4)\}$
  - 2: Solve  $\min\{(4.1\text{a}) : (4.1\text{g})\text{--}(4.1\text{p}), (4.2), (4.4)\}$  to obtain  $(a_{it}^*)$
  - 3: Compute  $\text{UBE} = \sum_{i \in \mathcal{B}} \sum_{t \in \mathcal{T}} e_{it} a_{it}^*$
  - 4: Generate a list size of  $n$  which consists numbers spaced on a logarithmic scale between LBE and UBE as  $\{\rho^1, \rho^2, \dots, \rho^n\}$
  - 5: **for**  $k = 1$  *to*  $n$  **do**
  - 6:      $\bar{E} = \rho_k$
  - 7:     Compute  $\text{LB}_k = \min\{(4.1\text{a}) : (4.1\text{g})\text{--}(4.1\text{q}), (4.2), (4.4)\}$  and obtain  $(a_{it}^*, b_{it}^*)$
  - 8:     **for all**  $t \in \mathcal{T}$  (in parallel) **do**
  - 9:         Fix  $p_i^d$  in (2.2) to  $p_i^d + a_{it}^* - \eta_i b_{it}^*$
  - 10:         Set an initial value for each variable
  - 11:         Solve model (2.2) to obtain  $\text{UB}_{kt}$
  - 12:      $\text{UB}_k = \sum_{t \in \mathcal{T}} \text{UB}_{kt}$
  - 13:     Compute  $\% \text{Gap} = 100 \times (1 - \text{LB}_k / \text{UB}_k)$
  - 14: Plot coordinates  $\{(\text{LB}_k, \rho_k) : k = 1, \dots, n\}$  and  $\{(\text{UB}_k, \rho_k) : k = 1, \dots, n\}$
- 

## 4.4 Input

In this section, we provide information on input datasets utilized for constructing the optimization model. Our aim is to use realistic datasets in order to suggest practical solutions to cope with possible grid challenges. Most of the researchers use synthetic grid data in OPF studies because access to confidential information on power grids is restricted, and actual grid data is not publicly available. Thus the existence of realistic grid data becomes more critical. In our study, we use a realistic synthetic test case and integrate real datasets to increase the applicability of the optimization model. In detail, our model draws on three real data sets: hourly electricity consumption, hourly marginal emission factors, and EV driving profiles. Therefore, we select the regions where a realistic OPF test case and real datasets are available. In the following sections, we explain these datasets and describe their variations across different regions. In Section 4.5.1, we will discuss in detail how to process these datasets.

### 4.4.1 OPF Test Case

The first important piece of information is the OPF test case. We test our algorithm on 200-bus, 500-bus, and 2000-bus Texas AM University (TAMU) instances from

the Power Grid Library (PGLIB-OPF) (Birchfield, Xu, Gegner, Shetye & Overbye, 2016), geographically situated in Illinois (IL), South Carolina (SC), and Texas (TX), respectively. These synthetic test cases do not match to any actual grid; they are constructed based on the statistical characteristics of the actual grid. The creators of these test cases initially situate substations in a specified region and determine loads and generators of these substations in such a way that generation and load profiles are similar to real profiles. Then, they link these substations with an automated line placement process based on realistic choices. They also consider additional complexities such as voltage control and transient stability to make the test cases more realistic. For detailed information on how to generate these test cases, see Birchfield et al. (2016). The main reason why we prefer to use TAMU instances is their similarity in size, complexity, and characteristics to real networks, in addition to the availability of real datasets given below for the same regions.

In the test cases used in this study, substations are situated in the central part of the IL, northwestern part of the SC and the whole state of TX. More details about the distribution networks are given in Table 4.1.

Table 4.1 Size of the instances.

Number of	TAMU Instances		
	IL	SC	TX
buses	200	500	2000
buses with demand	112	200	1125
lines	245	597	3206
generators	49	90	544

#### 4.4.2 Electricity Demand

Electricity demand is the second important piece of information. We retrieve the hourly electricity demand data available in Energy Information Administration EIA (2020). We match each test case with the demand data in the corresponding region. The hourly demand data for Illinois is not available, instead we consider the Mid-continent Independent System Operator’s demand. For SC and TX, we use demand for the SC Public Service Authority and regional demand of Texas.

Seasonal variations in electricity demand may result in differences in the operation scheduling of the network. Therefore, the numerical experiments are conducted using data both for a summer’s day and a winter’s day to demonstrate the influences

of the variations on the model results. To generate an *average* day, we first calculate the hourly averages of electricity consumption for a certain month. Then, these hourly averages are normalized by the maximum consumption as outlined in Algorithm 2 and plotted in Figure 4.1 for August 2018 and December 2018. We will explain how to process the normalized data to determine the real and reactive power demand of the grid in more detail in Section 4.5.1.

---

**Algorithm 2** Normalization

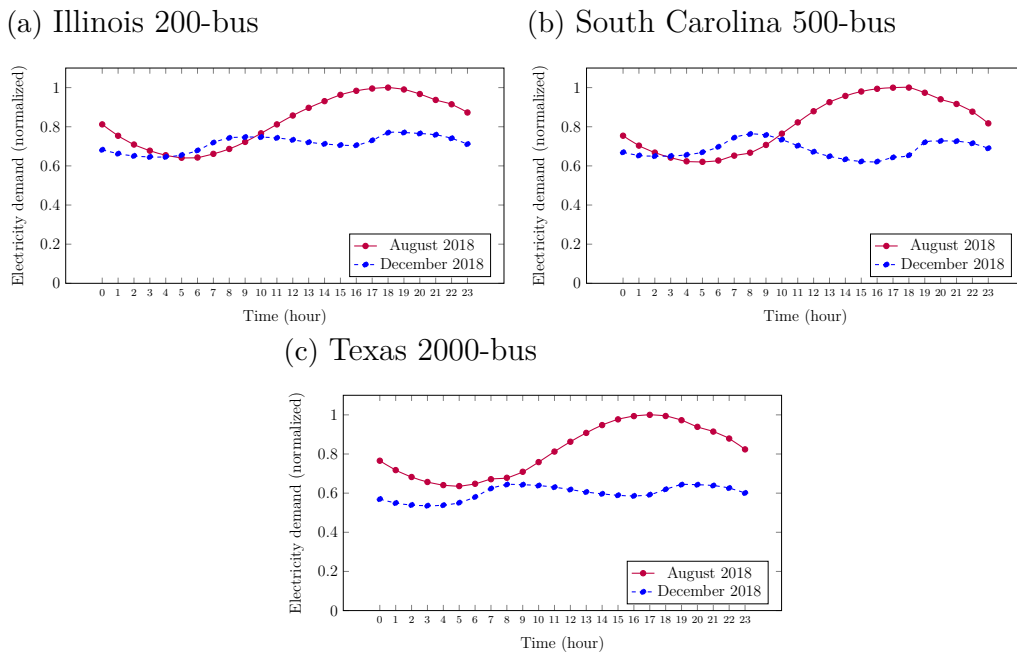
---

**Input:** Sets of hourly electricity demand for a summer’s day and a winter’s day:  $\mathcal{U} = \{u_t : t \in \mathcal{T}\}$  and  $\mathcal{W} = \{w_t : t \in \mathcal{T}\}$

**Output:**  $\bar{\mathcal{U}} = \{\bar{u}_t : t \in \mathcal{T}\}$  and  $\bar{\mathcal{W}} = \{\bar{w}_t : t \in \mathcal{T}\}$

- 1:  $\text{max\_consumption} = \max(\mathcal{U} \cup \mathcal{W})$
  - 2: **for all**  $t \in \mathcal{T}$  **do**
  - 3:      $\bar{u}_t = \frac{u_t}{\text{max\_consumption}}, \bar{w}_t = \frac{w_t}{\text{max\_consumption}}$
- 

Figure 4.1 Hourly electricity demand.

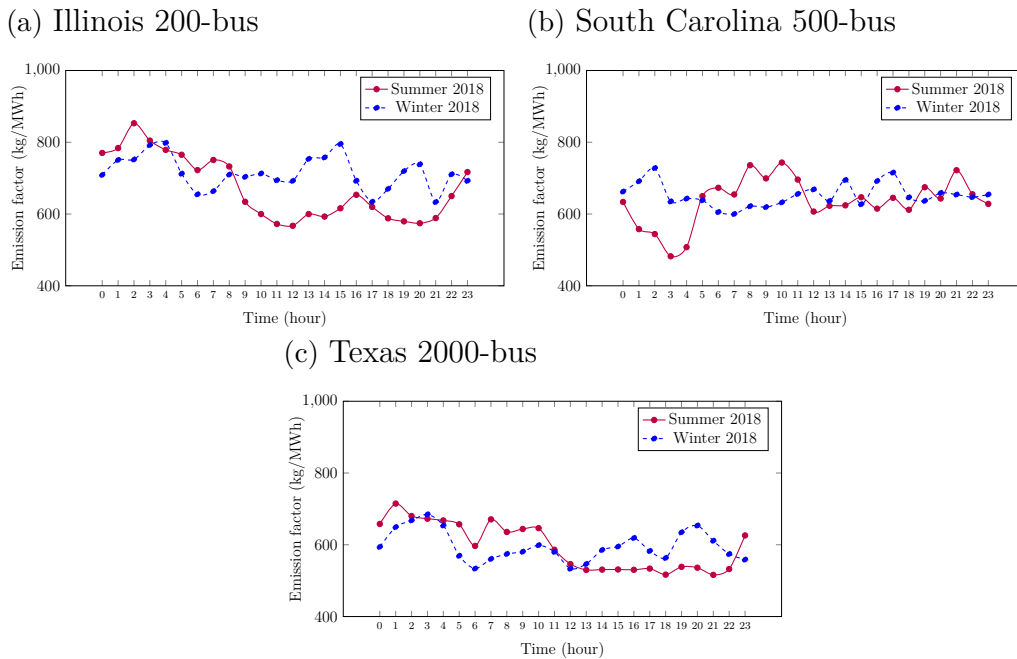


Hourly electricity consumption follow a similar trend across all regions. The total consumption in summer is higher than in winter. In winter, hourly electricity consumption varies slightly and peaks in the morning and the evening, while in summer it peaks in the afternoon.

### 4.4.3 Emission Factors

The other real dataset is the emission factors. We use the marginal emissions that occur from power stations to satisfy additional demand for EV charging. We retrieve marginal emission factors estimates, available in the Climate and Energy Decision Making Center by Azevedo IL (2019). We only take into account of CO<sub>2</sub> emissions and (although our framework would allow) do not investigate the effects of other air pollutants. For the winter and summer, the hourly marginal CO<sub>2</sub> emission factors in kg/MWh are shown in Figure 4.2.

Figure 4.2 Marginal CO<sub>2</sub> emission factors.



The marginal emission factors, as shown in Figure 4.2, vary widely across regions, seasons, and time.

### 4.4.4 Driving Profiles

Our model also considers driving profiles to determine charging profiles. We use the driving profiles over 24-hour that include energy requirement at time  $t$  and vehicle weight, which is the number of EVs using a certain driving profile. We explain in detail how to obtain these profiles in Algorithm 3. We use the National Household Travel Survey (NHTS) (NHTS, 2017) dataset, a household survey that tracks trends in personal travel and includes all transportation modes. The NHTS dataset con-

tains household, person, vehicle, and travel day trip files. We use vehicle and travel day trip files. The vehicle file includes records for each household vehicle, while the travel day trip file includes records for each personal trip. Regional data is available for IL, SC, and TX. We select trips made by a personal vehicle and eliminate non-household vehicles. We do not eliminate nonelectric vehicles to investigate how their electricity consumption will affect the OPF problem, if a portion of these vehicles becomes electric.

---

**Algorithm 3** Driving Profile

---

**Input:** Trip index  $r \in [0, R]$ , vehicle index  $v \in [0, V]$

From vehicle and travel day trip file import  $D_r$ : Total distance travelled during trip  $r$ ,  $S_r$ : Start time of trip  $r$ ,  $E_r$ : End time of trip  $r$ ,  $\mathcal{S}_v$ : Set of trips for vehicle  $v$ ,  $w_v$ : weight for vehicle  $v$

$c^{avg}$ : Average energy consumption per mile

$\bar{B}$ : Battery capacity

**Output:** Driving Profile

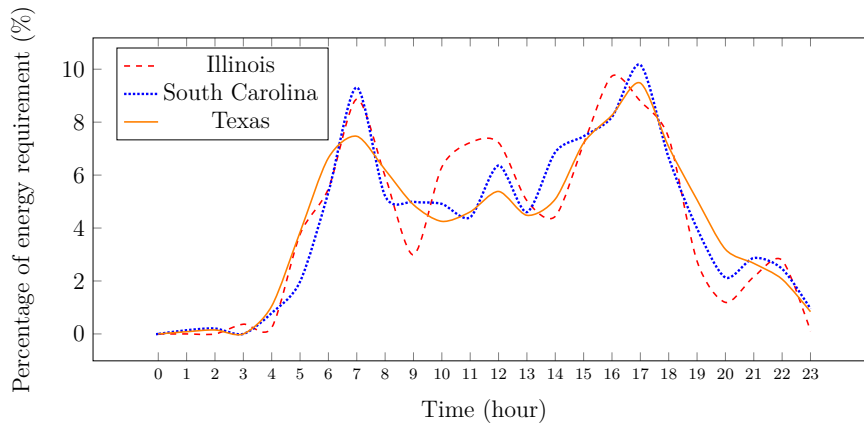
- 1: Select region
  - 2: Select passenger cars (Car, SUV, Van, Pickup Truck)
  - 3: Delete nonhousehold vehicles
  - 4: **if**  $D_r \geq \bar{B}/c^{avg}$  **then**
  - 5:     Delete trip  $r$
  - 6: Create a drive duration matrix  $\Delta$  of size  $T \times R$
  - 7: **for all**  $t \in [0, T], r \in [0, R]$  **do**
  - 8:     **if**  $S_r \leq t - 1$  **and**  $E_r \geq t$  **then**
  - 9:          $\Delta_{rt} = 60$
  - 10:     **if**  $S_r \geq t$  **or**  $E_r \leq t - 1$  **then**
  - 11:          $\Delta_{rt} = 0$
  - 12:     **else**
  - 13:          $\Delta_{rt} = \min(t, E_r) - \max(t - 1, S_r)$
  - 14: Calculate average speed  $S_r^{avg} = D_r / (E_r - S_r)$
  - 15: Create an EV energy consumption matrix  $\Omega$  of size  $T \times V$
  - 16: **for all**  $t \in [0, T], v \in [0, V]$  **do**
  - 17:      $\Omega_{vt} = \sum_{r \in \mathcal{S}_v} S_r^{avg} \Delta_{tr} c^{avg}$
  - 18: Driving profile of vehicle  $v$   $\Omega_v = \{\Omega_{vt} : t \in [0, T]\}$
- 

To obtain the energy requirement of vehicles at time  $t$ , we make some assumptions. Nissan Leaf has the highest sales in the moderate cost electric car segment in US INSIDEEVs (2020). Therefore, we assume all of the EVs are similar to Nissan Leaf. The standard battery of Nissan Leaf has usable capacity of 32 kWh, that is 80% of the its 40 kWh capacity (NISSAN, 2020); we set the battery capacity  $\bar{B}$  to 32. According to EPA (2020), this vehicle has an average energy consumption of 0.3 kWh/mile. We assume the energy consumption is constant and set the corresponding parameter  $c^{avg}$  to 0.3. Lastly, we also eliminate trips that require more than a full battery. After filtering the data, we calculate energy requirements at each time  $t$  for vehicle

$v$  as outlined in Algorithm 3. Vehicle weights  $w_v$  are already provided in datasets.

Since the data is only available for one typical day, we use the same EV driving profiles both summer and winter ignoring possible seasonal variations. Figure 4.3 provides an overview of these driving profiles. We will later explain how to process these driving profiles to integrate our model in detail in Section 4.5.1.

Figure 4.3 Percentage of energy requirement of EVs by time of day.



## 4.5 Computational Experiments

This section presents the results of our computational experiments, which have been conducted to investigate the effectiveness of our approach and assess the aggregate impact of EV charging load on optimal network operations under different scenarios. We first discuss the experimental setup to explain how we integrate input datasets in Section 4.4 into the MOPF model in Section 4.2. Then, we graphically illustrate the results of the computational experiments.

### 4.5.1 Experimental Setup

This section presents how we process input datasets so as to be compatible with the multi-period formulation. For the MOPF model, we consider a 24-hour period, in 1-hour slots, from 00:00 to 00:00 the following day.

The TAMU instances include network parameters for only one single period. Most

of the parameters remain constant throughout the day, but some parameters vary on an hourly basis such as power load and electricity price. To extend to the multi-period version, we multiply the real and reactive power load of the grid with the corresponding normalized values obtained from Algorithm 2 as follows:

$$p_{it}^d = p_i^d \times \bar{u}_t, \quad q_{it}^d = q_i^d \times \bar{u}_t \quad i \in \mathcal{B}, t \in \mathcal{T},$$

$$p_{it}^d = p_i^d \times \bar{w}_t, \quad q_{it}^d = q_i^d \times \bar{w}_t \quad i \in \mathcal{B}, t \in \mathcal{T}.$$

Here  $\bar{u}_t$  and  $\bar{w}_t$  are the normalized values for summer and winter seasons. Since hourly electricity price data is not publicly available for U. S. (EIA, 2020), we assume that the price is constant over the 24-hour period. We adjust emission parameters  $e_{it}$  to corresponding marginal emission factors in Section 4.4.3.

We utilize EV driving profiles to adjust parameter settings related to EV charging. We assume that EVs can only be charged at a bus with a nonzero real power load. If there is no real load at bus  $i$ , we set  $c_{it} = \bar{a}_{it} = \bar{b}_{it} = \bar{s}_{it} = \bar{v}_{it} = 0$  for all  $t \in \mathcal{T}$ .

Instead of individual EVs, we consider EV groups each containing EVs with the same driving profile. Some of these EV fleets are assigned to buses according to their weighted energy demand,  $\sum_{t \in \mathcal{T}} w_v \Omega_{vt}$ , in such a way that each bus  $i \in \mathcal{D}$  has one EV fleet. Assuming that if the bus load is high, the EV demand around the bus is also high; we assign an EV fleet with a higher demand to a bus with a higher load. The steps of the procedure used for this assignment are provided in Algorithm 4.

---

**Algorithm 4** Assignment

---

**Input:** *parameter*,  $\mathcal{BD} = \{p_i^d : i \in \mathcal{D} \subseteq \mathcal{B}\}$ ,  $\mathcal{EV} = \{\sum_{t \in \mathcal{T}} w_v \Omega_{vt} : v \in [0, V]\}$

**Output:** Assignment of EVs to buses

- 1: Sort  $\mathcal{BD}$  and  $\mathcal{EV}$  in ascending order
  - 2: Normalize  $\mathcal{BD}$  by  $\max(\mathcal{BD})$  and  $\mathcal{EV}$  by  $\max(\mathcal{EV})$
  - 3:  $k \leftarrow 0$
  - 4: **for all**  $n \in [0, \text{size}(\mathcal{BD})]$  **do**
  - 5:     **if**  $\text{parameter} * \mathcal{BD}[n] \geq \mathcal{EV}[k]$  **then**
  - 6:         Assign EV in the  $k$ th order of  $\mathcal{EV}$  to the  $n$ th bus in  $\mathcal{BD}$
  - 7:          $k \leftarrow k + 1$
  - 8:     **else**
  - 9:         **for**  $j \in [n, \text{size}(\mathcal{EV})]$  **do**
  - 10:             **if**  $\mathcal{BD}[n] > \mathcal{EV}[j]$  **then**
  - 11:                 Assign EV in the  $j$ th order of  $\mathcal{EV}$  to the  $n$ th bus in  $\mathcal{BD}$
  - 12:                  $k \leftarrow j + 1$
  - 13:             **break**
- 

Now, each bus with a real power load has one fleet of EV, and thus we can use bus

indices  $i$  instead of vehicle indices  $v$  for brevity. We adjust parameter settings for EV fleets instead of individual EVs. We first set energy requirements  $c_{it}$  to  $w_i\Omega_{it}$  for  $i \in \mathcal{D}, t \in \mathcal{T}$ . According to the energy requirements, we determine stock parameter  $s_{it}$  for each period. If an EV has demand during successive periods  $(t, t+1, \dots, t+n)$ , the amount of battery charge at the beginning of the period  $t$  should be sufficient to satisfy the demand in these successive periods. In regard to this, the stock parameters are determined as in Algorithm 5.

---

**Algorithm 5** Stock parameter settings of EV at bus  $i$

---

**Input:**  $\{c_{it} : t \in \mathcal{T}\}$

**Output:**  $\{s_{it} : t \in \mathcal{T}\}$

```

1:  $s_{it} = 0$  for all  $t \in \mathcal{T}$ 
2:  $t = 1$ 
3: while  $t \leq T$  do
4:   if  $c_{it} \neq 0$  then
5:      $k \leftarrow t$ 
6:     while  $c_{ik} \neq 0$  and  $t \leq T$  do
7:        $s_{i(t-1)} \leftarrow s_{i(t-1)} + c_{ik}$ 
8:        $k \leftarrow k + 1$ 
9:      $t \leftarrow k$ 

```

---

As previously mentioned in Section 4.4.4, we use the Nissan Leaf as a baseline vehicle. The Nissan Leaf has a usable battery capacity of 32kWh with a 6.6kW onboard charger (NISSAN, 2020). We assume that charging rates are constant over a period. For each bus  $i \in \mathcal{D}$ , the maximum limit of charging and discharging powers,  $\bar{a}_{it}$  and  $\bar{b}_{it}$ , is set to  $w_i \times 6.6$ . We set the stock parameter  $\bar{s}_{it}$  to usable battery capacity, that is  $w_i \times 32$ , and the charging efficiency to 98% (Zhang, Yigang, Mingjian & Yongling, 2017). We consider two different settings for the initial battery state of charge (SOC) at the beginning of the day. In the first case, the initial battery SOC  $I_i$  is equal to zero for each  $i \in \mathcal{D}$ . In the second case, for each EV, we first find the maximum possible level of battery charge (in percentage) at the end of the day. Then, we set the initial battery SOC  $I_i$  for EV at bus  $i \in \mathcal{D}$  to this computed value. The second setting adds some flexibility to initial battery SOC of EVs.

To make the ratio of the electricity consumption and EV charging demand consistent with the actual data, we calculate a parameter called **weight** as the ratio between the total power demand of the grid and daily electricity consumption as follows:

$$(4.5) \quad \text{weight} = \frac{\sum_{i \in \mathcal{B}} \sum_{t \in \mathcal{T}} p_{it}^d}{\max(\sum_{t \in \mathcal{T}} u_t, \sum_{t \in \mathcal{T}} w_t)}.$$

Here,  $u_t$  and  $w_t$  are the electricity consumptions for summer and winter obtained from Algorithm 2. We multiply EV charging requirement  $c_{it}$  and thereby all charging



parameters  $\bar{a}_{it}, \bar{b}_{it}, \underline{s}_{it}, \bar{s}_{it}, I_i$  with **weight**. Note that we use the same **weight** for different seasons. Table 4.2 summaries the daily demand data at a macro level.

Table 4.2 Daily demands in kWh.

	Region			Source
	IL	SC	TX	
August demand ( $\sum_{t \in \mathcal{T}} u_t$ )	149690	82575	1256288	Algorithm 2
December demand ( $\sum_{t \in \mathcal{T}} w_t$ )	129297	69901	923604	Algorithm 2
Grid demand ( $\sum_{i \in \mathcal{B}} p_i^d$ )	1476	7751	67109	Model (2.2)
Total grid demand ( $\sum_{i \in \mathcal{B}} \sum_{t \in \mathcal{T}} p_{it}^d$ )	29276	151214	1313994	Model (4.1)
EV demand ( $\sum_{t \in \mathcal{T}} \sum_{v \in \mathcal{V}} \Omega_{vt} w_v$ )	9632	3312	22646	Algorithm 3
<b>weight</b>	0.19	1.83	1.05	Equation (4.5)

We assume that an EV cannot be driven and connected to the grid in the same period. If the EV is in driving mode at time  $t$ , we set  $a_{it}$  and  $b_{it}$  to be zero. If EV has no energy requirement at time  $t$ , we assume that it is connected to the grid, and optimization decides exactly one mode among the following three based on the driving profile: charging, discharging, or rest mode. It can only be in one of these modes during time  $t$ . In addition, if the operating cost of a generator is zero, then we remove the lower bound on the power generation and set  $\bar{p}_i = 0$ .

The proposed MOPF model allows bidirectional flow, from grid to vehicle (G2V) and vehicle to grid (V2G). In the case where only unidirectional flow G2V is allowed, the maximum allowable discharging rate  $\bar{b}_{it}$  should be set to zero.

#### 4.5.2 Results and Discussion

In this section, we report the result of our computational experiments on the instances from PGLIB-OPF. A 64-bit desktop with Intel Core i7 CPU with 3.20GHz processor and 64 GB RAM is used for all experiments. Our code is written in Python programming language using Spyder environment. The solvers GUROBI and IPOPT are used to solve the SOCP relaxation and the NLP models, respectively. In order to reduce the computational time, the NLP models are solved in parallel. We also set the initial value of each variable to the average of its upper and lower bounds.

We perform the optimization under different settings and illustrate eight cases for each of the regions depending on the season of the year, initial battery SOC, and direction of flow. Table 4.3 gives a summary of the input data and parameter settings for case studies.

Table 4.3 Input data and parameter settings.

Settings	
Region	Illinois South Carolina Texas
Season	Winter Summer
Initial battery SOC	0% max%
Direction of flow	only G2V G2V and V2G

For every combination of parameter settings, i.e., for 24 different cases, we run Algorithm 1. To illustrate the results, we group the test cases that belong to the same region and season. Each group consists of four different cases in the combination of the direction of flow and initial SOC settings. We plot results with both total generation cost and marginal generation cost in Figures 4.4–4.15.

#### 4.5.2.1 Computational Accuracy in Terms of Optimality Gap

To demonstrate the computational accuracy of the proposed optimization algorithm, we repeat Algorithm 1 and plot the results in Figures 4.4, 4.6, 4.8, 4.10, 4.12, and 4.14. These figures show lower bound (in red dashed line) obtained from SOCP relaxation and upper bounds (in solid blue line) computed via NLP models. These figures better illustrate the quality of our approach in terms of the optimality gap.

For the 200-bus system in IL and 2000-bus system in TX, the proposed approach is capable of providing approximately globally optimal solutions with an optimality gap below 0.005% and 0.7%, respectively. For the 500-bus system in SC, the optimality gaps are no more than 2.9% in winter; however, in summer, the optimality gaps vary between 3.9 % and 6.4 %. The authors in Babaeinejadsarookolae, Birchfield, Christie, Coffrin, DeMarco, Diao, Ferris, Fliscounakis, Greene, Huang & others (2019) also note that the 500-bus case exhibits a significant SOCP optimality gap. Overall, our proposed algorithm achieves relatively small percentage optimality gaps for all the instances we consider.

### 4.5.2.2 Marginal Cost vs. Marginal Emission

We also consider the marginal generation cost associated with the power generation of the grid for EV charging. We calculate marginal costs by subtracting the current cost, which is the optimal total cost of electricity without EV charging load, from the total generation cost. Figures 4.5, 4.7, 4.9, 4.11, 4.13, and 4.15 may give a better understanding of the relation between cost and emission.

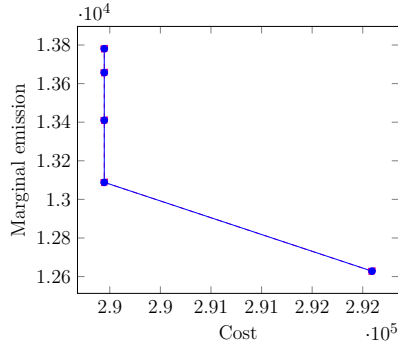
Figures 4.4–4.7 depict different cases for Illinois. These graphs show how marginal emission and cost change in relation to each other. At first sight, one can easily observe that marginal emission and marginal cost are inversely correlated. When we set tight restrictions on marginal emission, the marginal cost tends to rise while we aim to minimize marginal cost, marginal emission increases. In some cases, despite the tighter restrictions on marginal emission, the marginal cost remains the same up to a point. At this point, the reduction of marginal emission is *free*. For example, in Figure 4.5a with no change in the generation cost, marginal emission decreases by approximately 6%.

### 4.5.2.3 Effect of V2G

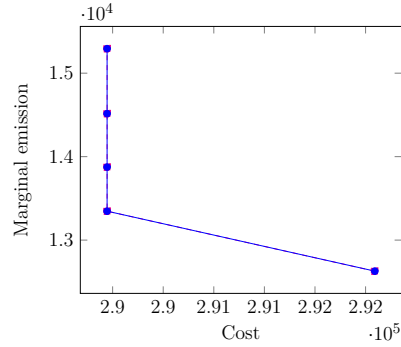
We investigate how marginal emissions and marginal costs are affected by the integration of the V2G concept. The bidirectional flow has the potential to decrease marginal cost. For example, we observe negative marginal costs in Figure 4.7b. In the case of bidirectional flow (see Figure 4.17e), EVs are charged during off-peak hours of electricity consumption and give energy back to the grid during peak hours to reduce the peak load of the power grid. This results in a reduction of power losses, thereby decreasing the total generation cost. However, this phenomenon does not only depend on the direction of flow but also the initial SOC setting. When the final battery SOC should be equal to max % at the end of the day, there is no reduction in the peak load of the grid (see Figure 4.17g), and thus the generation cost remains the same as in unidirectional flow (see Figure 4.17c). We also observe similar results for the test cases in SC and TX, see Figures 4.11b and 4.15b.

Figure 4.4 Pareto frontier of total cost and marginal emission for Illinois (200-bus system) in winter.

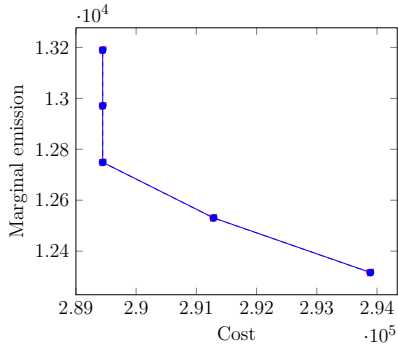
(a) SOC=0%, only G2V



(b) SOC=0%, G2V and V2G



(c) SOC=max%, only G2V



(d) SOC=max%, G2V and V2G

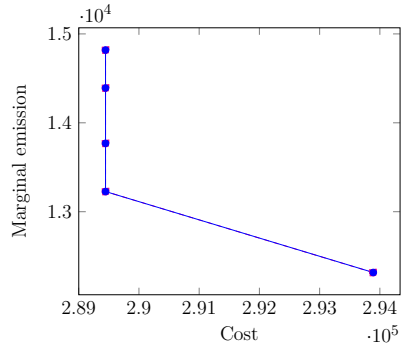
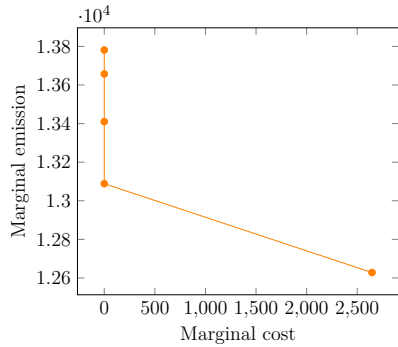
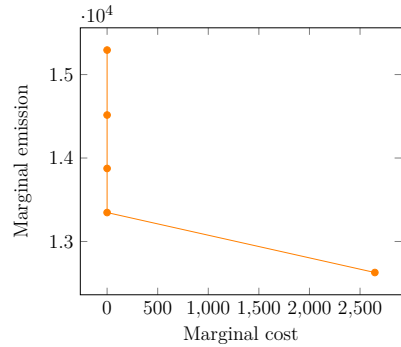


Figure 4.5 Pareto frontier of marginal cost and marginal emission for Illinois (200-bus system) in winter.

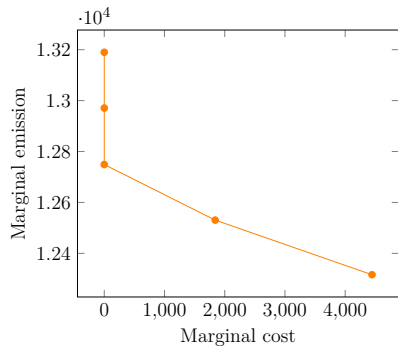
(a) SOC=0%, only G2V



(b) SOC=0%, G2V and V2G



(c) SOC=max%, only G2V



(d) SOC=max%, G2V and V2G

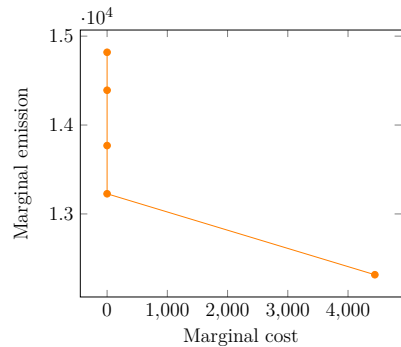
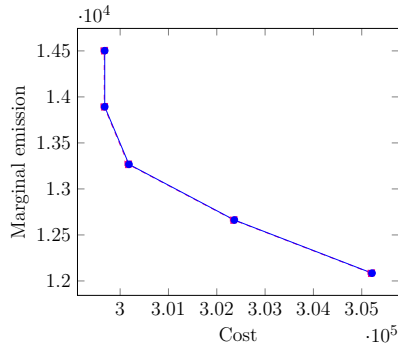
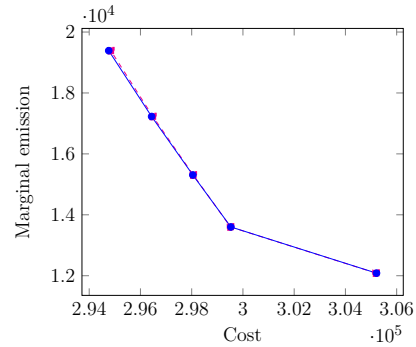


Figure 4.6 Pareto frontier of total cost and marginal emission for Illinois (200-bus system) in summer.

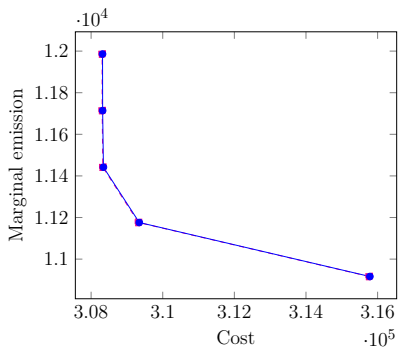
(a) SOC=0%, only G2V



(b) SOC=0%, G2V and V2G



(c) SOC=max%, only G2V



(d) SOC=max%, G2V and V2G

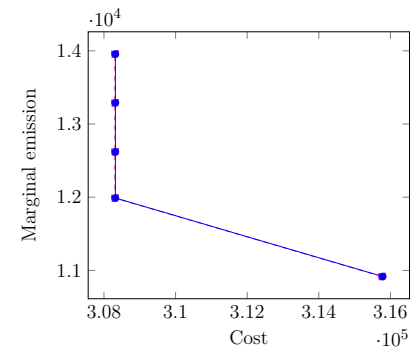
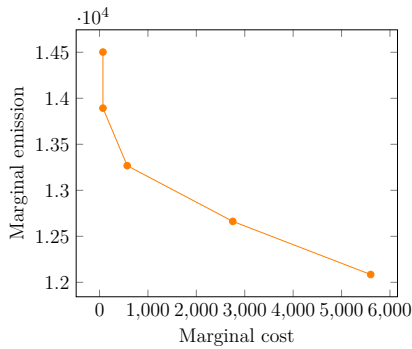
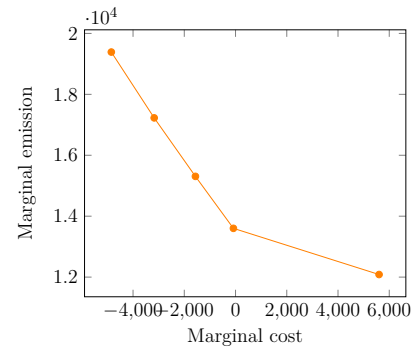


Figure 4.7 Pareto frontier of marginal cost and marginal emission for Illinois (200-bus system) in summer.

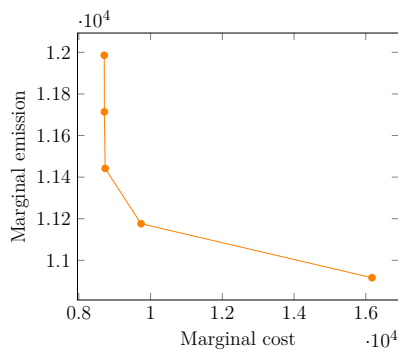
(a) SOC=0%, only G2V



(b) SOC=0%, G2V and V2G



(c) SOC=max%, only G2V



(d) SOC=max%, G2V and V2G

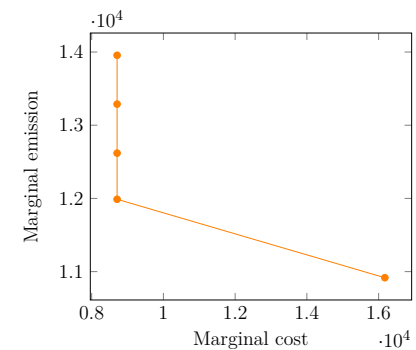
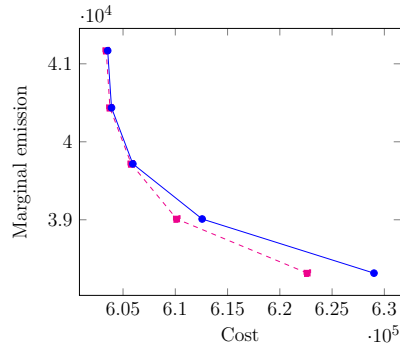
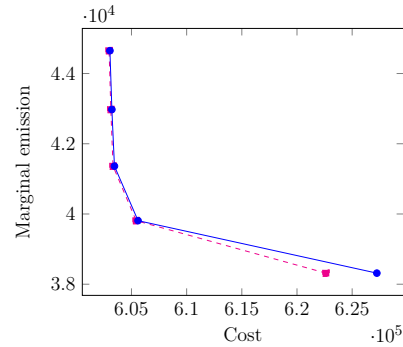


Figure 4.8 Pareto frontier of total cost and marginal emission for South Carolina (500-bus system) in winter.

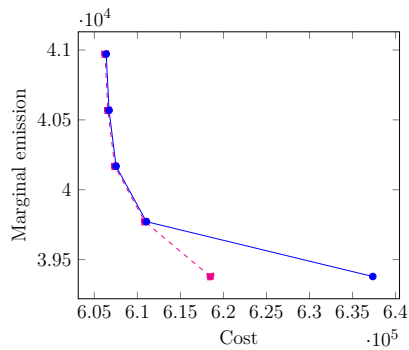
(a) SOC=0%, only G2V



(b) SOC=0%, G2V and V2G



(c) SOC=max%, only G2V



(d) SOC=max%, G2V and V2G

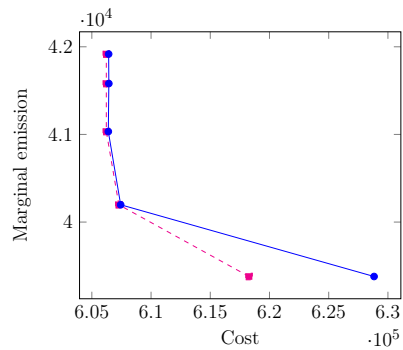
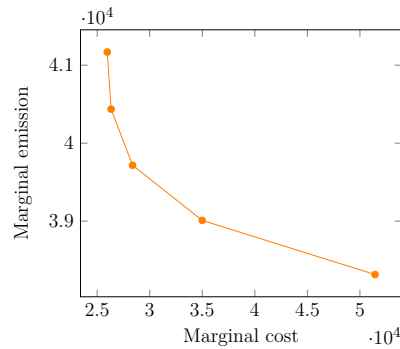
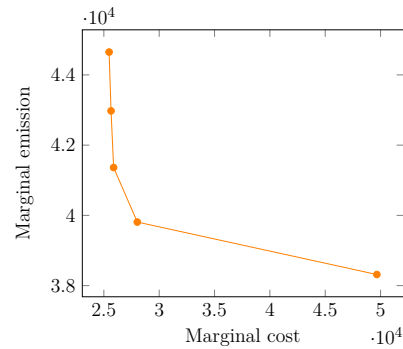


Figure 4.9 Pareto frontier of marginal cost and marginal emission for South Carolina (500-bus system) in winter.

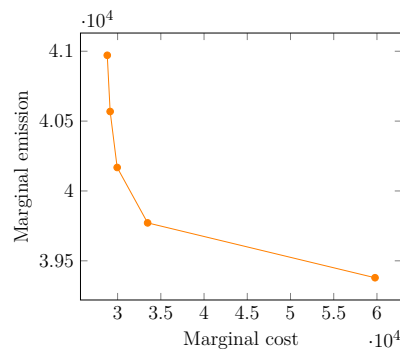
(a) SOC=0%, only G2V



(b) SOC=0%, G2V and V2G



(c) SOC=max%, only G2V



(d) SOC=max%, G2V and V2G

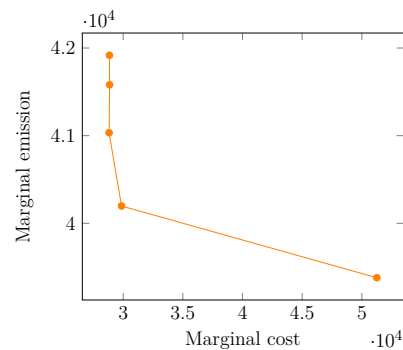
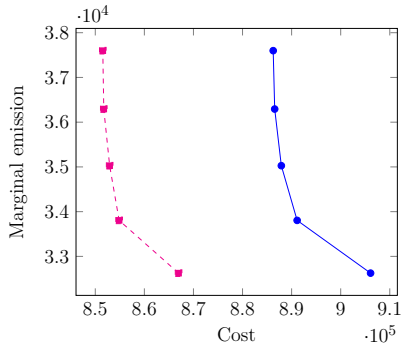
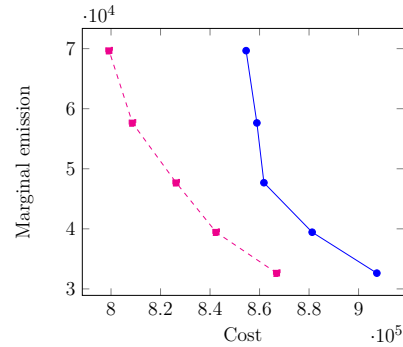


Figure 4.10 Pareto frontier of total cost and marginal emission for South Carolina (500-bus system) in summer.

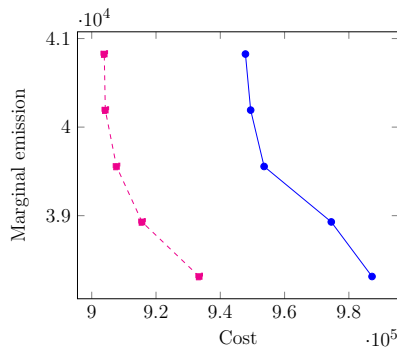
(a) SOC=0%, only G2V



(b) SOC=0%, G2V and V2G



(c) SOC=max%, only G2V



(d) SOC=max%, G2V and V2G

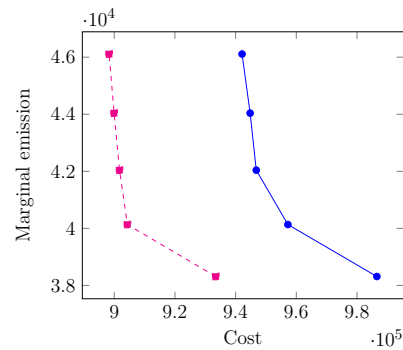
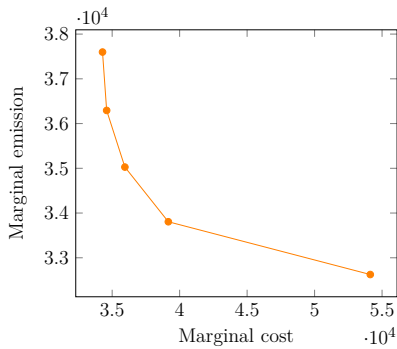
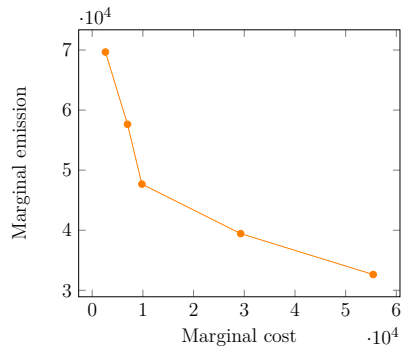


Figure 4.11 Pareto frontier of marginal cost and marginal emission for South Carolina (500-bus system) in summer.

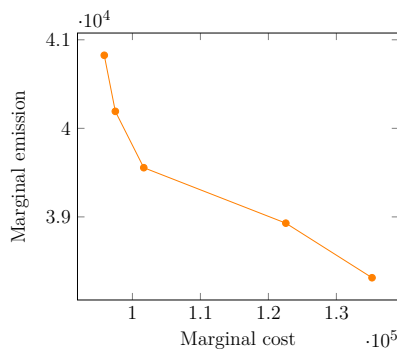
(a) SOC=0%, only G2V



(b) SOC=0%, G2V and V2G



(c) SOC=max%, only G2V



(d) SOC=max%, G2V and V2G

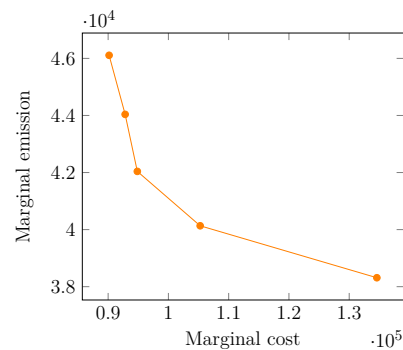
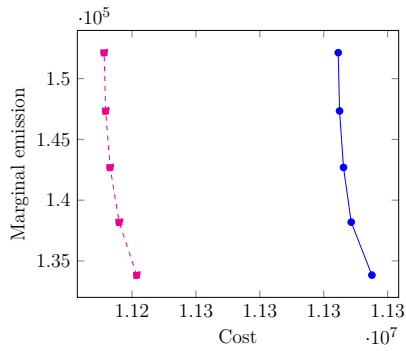
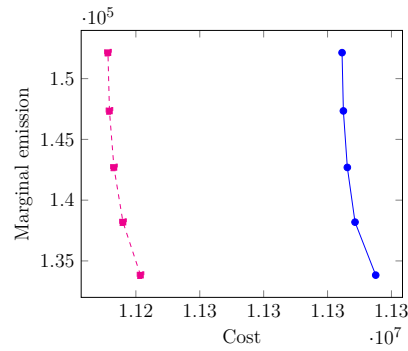


Figure 4.12 Pareto frontier of total cost and marginal emission for Texas (2000-bus system) in winter.

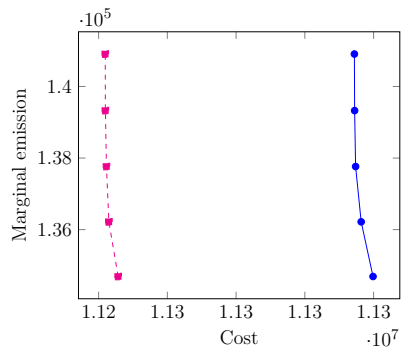
(a) SOC=0%, only G2V



(b) SOC=0%, G2V and V2G



(c) SOC=max%, only G2V



(d) SOC=max%, G2V and V2G

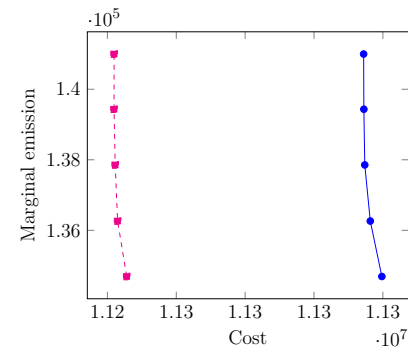
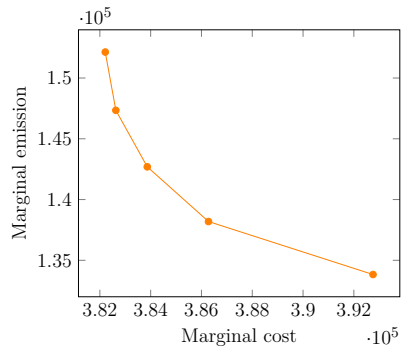
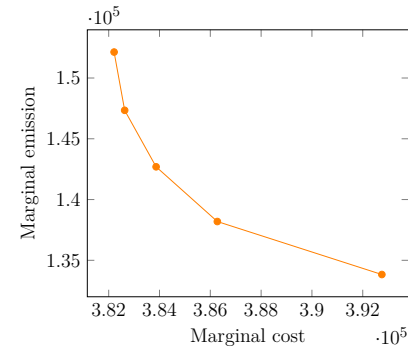


Figure 4.13 Pareto frontier of marginal cost and marginal emission for Texas (2000-bus system) in winter.

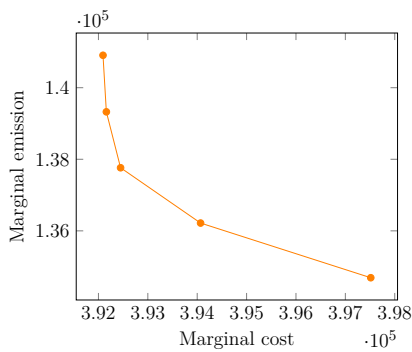
(a) SOC=0%, only G2V



(b) SOC=0%, G2V and V2G



(c) SOC=max%, only G2V



(d) SOC=max%, G2V and V2G

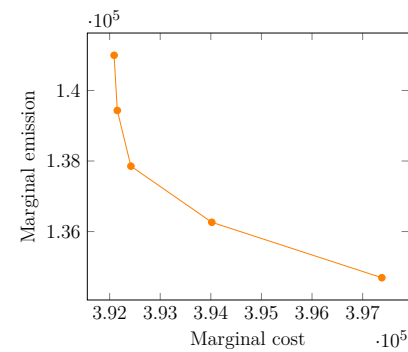
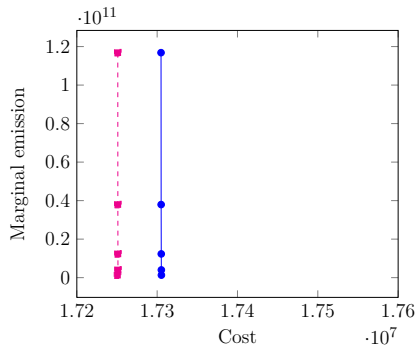


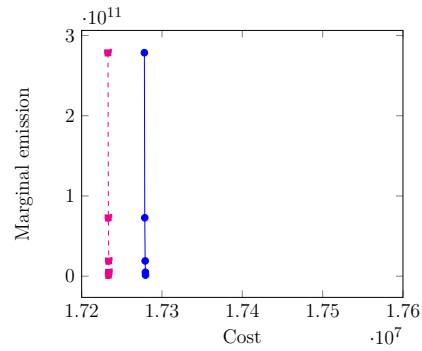


Figure 4.14 Pareto frontier of total cost and marginal emission for Texas (2000-bus system) in summer.

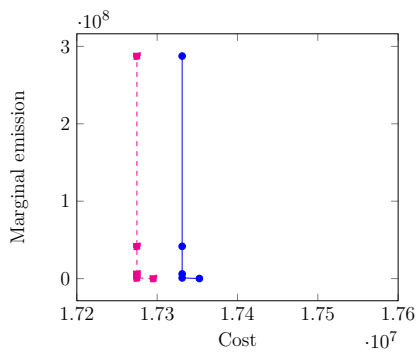
(a) SOC=0%, only G2V



(b) SOC=0%, G2V and V2G



(c) SOC=max%, only G2V



(d) SOC=max%, G2V and V2G

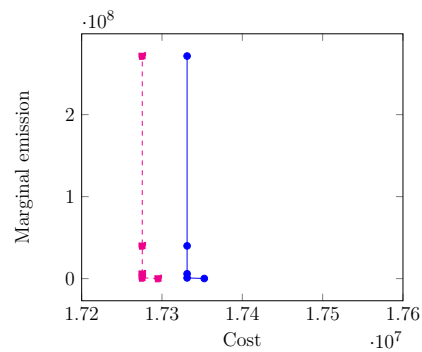
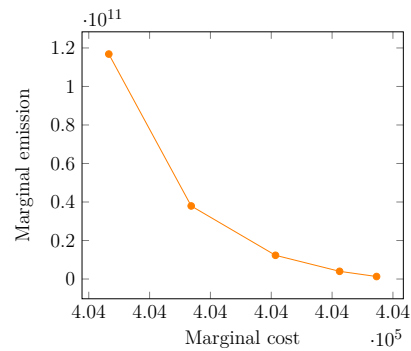
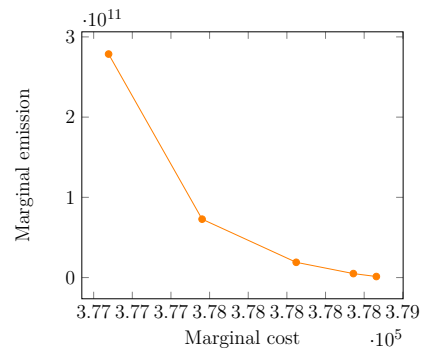


Figure 4.15 Pareto frontier of marginal cost and marginal emission for Texas (2000-bus system) in winter.

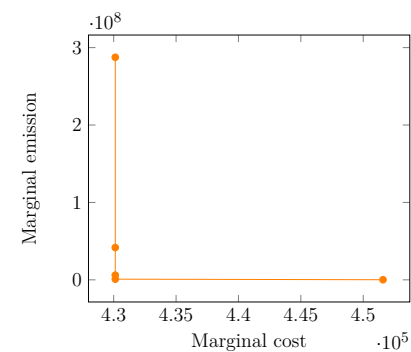
(a) SOC=0%, only G2V



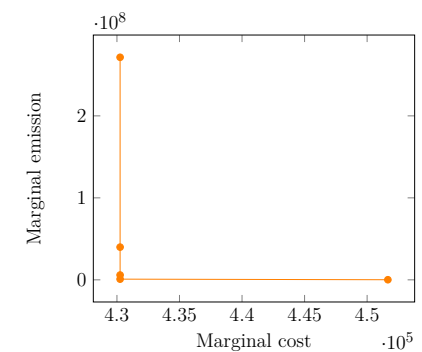
(b) SOC=0%, G2V and V2G



(c) SOC=max%, only G2V



(d) SOC=max%, G2V and V2G



#### 4.5.2.4 Hourly Load Variations for Illinois 200-Bus System

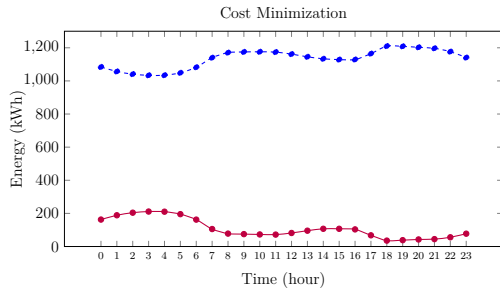
We also plot the conventional load without EVs (in dashed blue line), and EV charging load (in solid red line) and V2G power profile (in orange dotted line) power curves for both cost and emission minimization objectives in Figures 4.16 and 4.17. Because we observe similar trends for regions IL, SC, and TX in general, we only provide the plots for IL 200-bus system. Now, we will further analyze the effects of hourly electricity consumption and marginal emission factors on operations.

The curve trend of the EV charging load is opposite to that of conventional load without EVs under the cost minimization objective. For example, in Figure 4.17a, when the conventional load is relatively low early in the morning, the EV charging load is high while at the peak of the conventional load, the total EV charging load is minimal. On the other hand, EVs supply power to the grid at the peak of the conventional load in order to flatten the load profile (see Figure 4.17e).

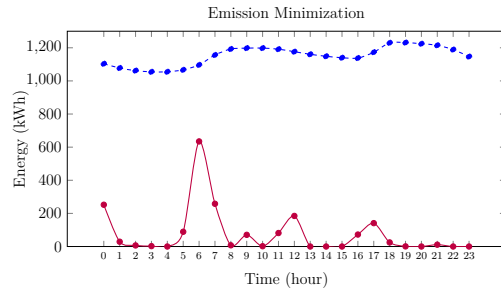
If the problem aims to minimize emission, the power grid generates electricity when the emission factor is relatively low, even at the peak of conventional load (see Figure 4.17h). This results in higher peaks of the grid; therefore, grid losses and consequently, total generation cost increases. It is also important to consider the impacts of initial SOC settings and driving profiles. For example in Figure 4.17b, although emission factors are higher in the early morning, EVs have to be charged in the early morning to satisfy their demand in the morning (see Figure 4.3).

Figure 4.16 Hourly load variations for Illinois (200-bus system) in winter.

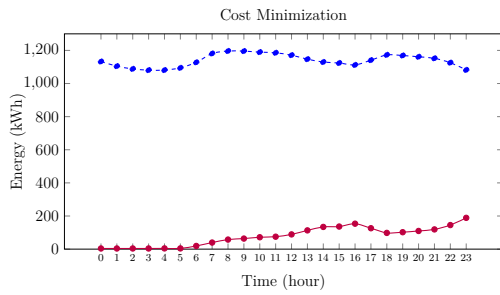
(a) SOC=0%, only G2V



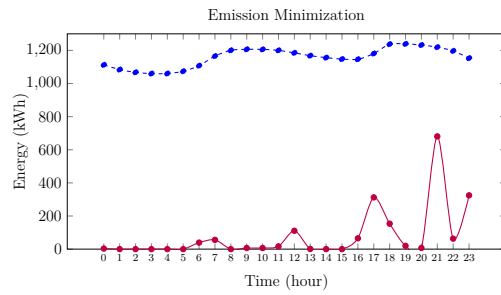
(b) SOC=0%, only G2V



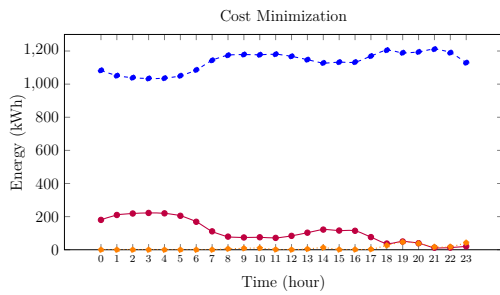
(c) SOC=max%, only G2V



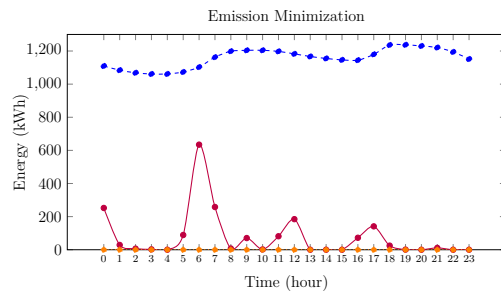
(d) SOC=max%, only G2V



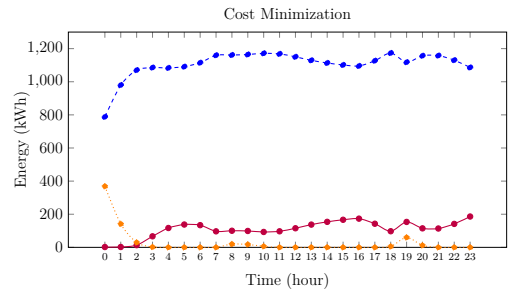
(e) SOC=0%, G2V and V2G



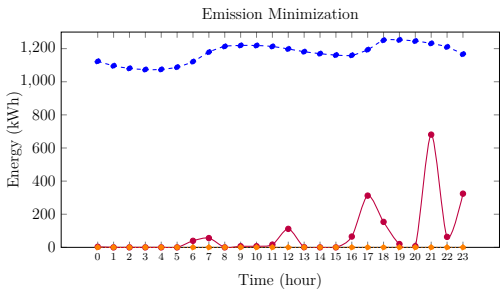
(f) SOC=0%, G2V and V2G



(g) SOC=max%, G2V and V2G



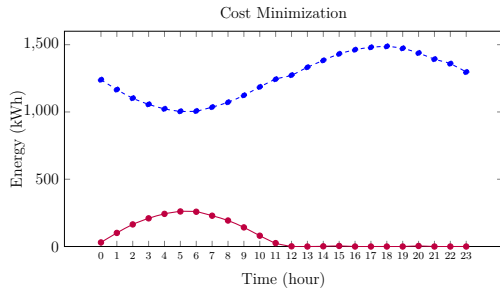
(h) SOC=max%, G2V and V2G



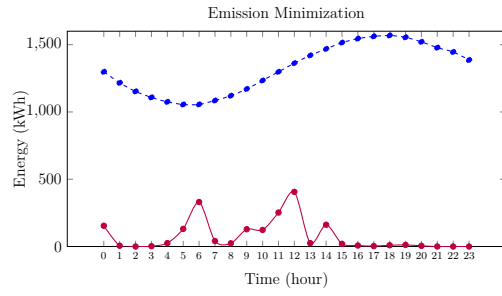
● EV charging load  
● V2G power profile  
● Conventional load without EVs

Figure 4.17 Hourly load variations for Illinois (200-bus system) in summer.

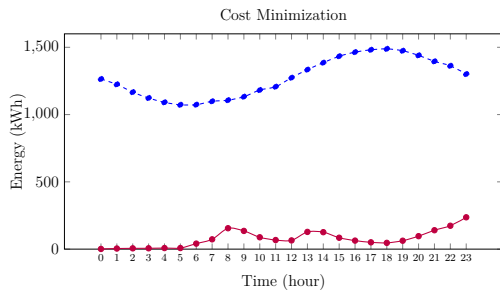
(a) SOC=0%, only G2V



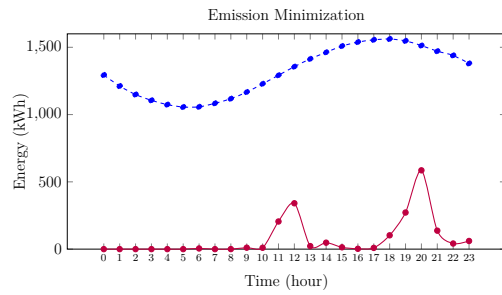
(b) SOC=0%, only G2V



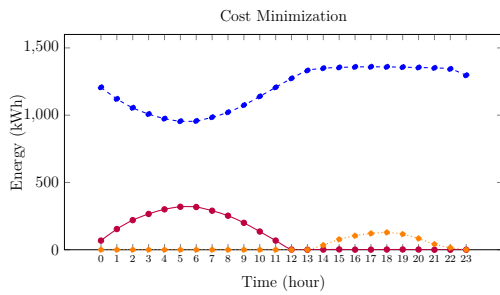
(c) SOC=max%, only G2V



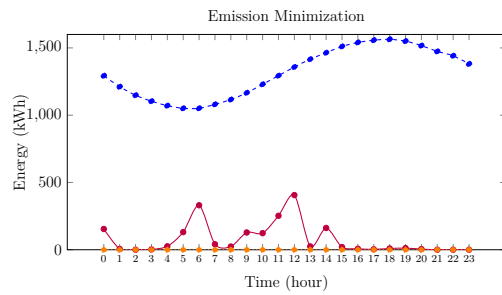
(d) SOC=max%, only G2V



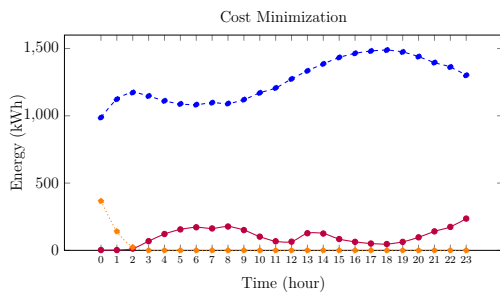
(e) SOC=0%, G2V and V2G



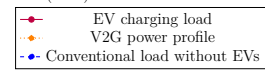
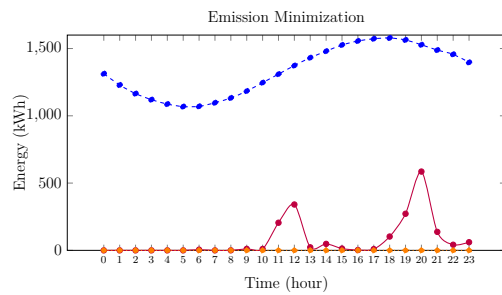
(f) SOC=0%, G2V and V2G



(g) SOC=max%, G2V and V2G



(h) SOC=max%, G2V and V2G



## 4.6 Conclusions

This chapter presents a solution approach based on SOCP to solve the multi-period joint OPF and EV charging problems. We propose a new mathematical formulation of the problem and its SOCP relaxation. We consider a realistic OPF test case with three real datasets: hourly electricity consumption, hourly marginal emission factor, and EV driving profiles. We systematically solve the SOCP and the original problem to approximate globally optimal solutions. We conduct computational experiments to investigate the aggregate effect of the EV charging load on the grid. A number of assumptions and limitations in the optimization model should be considered when interpreting our findings, such as constant electricity prices, the same EV type and constant charging rates. In addition, our model requires hourly electricity consumptions, EV charging demands, and charging location of each EV to be known a priori. Computational experiments on different sizes of OPF instances from PGLIB-OPF library show that our solution approach provides globally optimal solutions with minimal optimality gaps. In addition, through coordinated charging of EVs, marginal emission can be significantly reduced with no change or minimal increase in cost, and the integration of the V2G concept leads to cost savings, although assuming hourly electricity prices are constant.

## BIBLIOGRAPHY

- Abido, M. A. (2002). Optimal power flow using particle swarm optimization. *International Journal of Electrical Power & Energy Systems*, 24(7), 563–571.
- Acha, S., Green, T. C., & Shah, N. (2010). Effects of optimised plug-in hybrid vehicle charging strategies on electric distribution network losses. In *IEEE PES T&D 2010*, (pp. 1–6). IEEE.
- Acha, S., Green, T. C., & Shah, N. (2011). Optimal charging strategies of electric vehicles in the uk power market. In *ISGT 2011*, (pp. 1–8). IEEE.
- AFDC (2017). State alternative fuel and advanced vehicle laws and incentives: 2017 year in review by alternative fuels data center. <https://afdc.energy.gov/laws/>.
- Alonso, M., Amaris, H., Germain, J. G., & Galan, J. M. (2014). Optimal charging scheduling of electric vehicles in smart grids by heuristic algorithms. *Energies*, 7(4), 2449–2475.
- AlRashidi, M. & El-Hawary, M. (2009). Applications of computational intelligence techniques for solving the revived optimal power flow problem. *Electric Power Systems Research*, 79(4), 694–702.
- Andersson, S.-L., Elofsson, A., Galus, M. D., Göransson, L., Karlsson, S., Johnsson, F., & Andersson, G. (2010). Plug-in hybrid electric vehicles as regulating power providers: Case studies of sweden and germany. *Energy policy*, 38(6), 2751–2762.
- Azevedo IL, Donti PL, H. N. S. G. S.-E. K. V. P. (2019). Electricity marginal factor estimates by center for climate and energy decision making pittsburgh: Carnegie mellon university. <http://cedmcenter.org>.
- Azizipanah-Abarghooee, R., Terzija, V., Golestaneh, F., & Roosta, A. (2016). Multiobjective dynamic optimal power flow considering fuzzy-based smart utilization of mobile electric vehicles. *IEEE Transactions on Industrial Informatics*, 12(2), 503–514.
- Babaeinejadsarookolae, S., Birchfield, A., Christie, R. D., Coffrin, C., DeMarco, C., Diao, R., Ferris, M., Fliscounakis, S., Greene, S., Huang, R., et al. (2019). The power grid library for benchmarking ac optimal power flow algorithms. *arXiv preprint arXiv:1908.02788*.
- Bai, X., Wei, H., Fujisawa, K., & Wang, Y. (2008). Semidefinite programming for optimal power flow problems. *International Journal of Electrical Power & Energy Systems*, 30(6-7), 383–392.
- Bakirtzis, A. G., Biskas, P. N., Zoumas, C. E., & Petridis, V. (2002). Optimal power flow by enhanced genetic algorithm. *IEEE Transactions on Power Systems*, 17(2), 229–236.
- Bingane, C., Anjos, M. F., & Le Digabel, S. (2019). Tight-and-cheap conic relaxation for the optimal reactive power dispatch problem. *IEEE Trans. on Power Syst.*, 34(6), 4684–4693.
- Birchfield, A. B., Xu, T., Gegner, K. M., Shetye, K. S., & Overbye, T. J. (2016). Grid structural characteristics as validation criteria for synthetic networks. *IEEE Transactions on power systems*, 32(4), 3258–3265.
- Bukhsh, W. A., Grothey, A., McKinnon, K. I., & Trodden, P. A. (2013). Local

- solutions of the optimal power flow problem. *IEEE Transactions on Power Systems*, 28(4), 4780–4788.
- Cain, M. B., O’neill, R. P., & Castillo, A. (2012). History of optimal power flow and formulations. *Federal Energy Regulatory Commission*, 1, 1–36.
- Capitanescu, F., Glavic, M., Ernst, D., & Wehenkel, L. (2007). Interior-point based algorithms for the solution of optimal power flow problems. *Electric Power systems research*, 77(5-6), 508–517.
- Capitanescu, F. & Wehenkel, L. (2010). Sensitivity-based approaches for handling discrete variables in optimal power flow computations. *IEEE Trans. on Power Syst.*, 25(4), 1780–1789.
- Carpentier, J. (1962). Contribution to the economic dispatch problem. *Bulletin de la Societe Francoise des Electriciens*, 3(8), 431–447.
- Chen, N., Tan, C. W., & Quek, T. Q. S. (2014). Electric vehicle charging in smart grid: Optimality and valley-filling algorithms. *IEEE Journal of Selected Topics in Signal Processing*, 8(6), 1073–1083.
- Chiang, H.-D., Wang, B., & Jiang, Q.-Y. (2009). Applications of trust-tech methodology in optimal power flow of power systems. In *Optimization in the Energy Industry* (pp. 297–318). Springer.
- Clement-Nyns, K., Haesen, E., & Driesen, J. (2009). The impact of charging plug-in hybrid electric vehicles on a residential distribution grid. *IEEE Transactions on power systems*, 25(1), 371–380.
- Coffrin, C., Hijazi, H. L., & Van Hentenryck, P. (2015a). Distflow extensions for ac transmission systems. *arXiv preprint arXiv:1506.04773*.
- Coffrin, C., Hijazi, H. L., & Van Hentenryck, P. (2015b). The qc relaxation: A theoretical and computational study on optimal power flow. *IEEE Transactions on Power Systems*, 31(4), 3008–3018.
- EIA (2020). Hourly electricy consumption data by united states energy information administration. <http://https://www.eia.gov/beta/electricity/gridmonitor/>.
- El-Abiad, A. H. & Jaimes, F. J. (1969). A method for optimum scheduling of power and voltage magnitude. *IEEE Transactions on Power Apparatus and Systems*, (4), 413–422.
- EPA (2020). Nissan leaf’s average energy consumption by united states environmental protection agency. <https://fueleconomy.gov/>.
- Expósito, A. G. & Ramos, E. R. (1999). Reliable load flow technique for radial distribution networks. *IEEE Transactions on Power Systems*, 14(3), 1063–1069.
- Fan, H., Duan, C., Zhang, C.-K., Jiang, L., Mao, C., & Wang, D. (2017). Admm-based multiperiod optimal power flow considering plug-in electric vehicles charging. *IEEE Transactions on Power Systems*, 33(4), 3886–3897.
- Farivar, M., Clarke, C. R., Low, S. H., & Chandy, K. M. (2011). Inverter var control for distribution systems with renewables. In *2011 IEEE international conference on smart grid communications (SmartGridComm)*, (pp. 457–462). IEEE.
- Frank, S., Steponavice, I., & Rebennack, S. (2012). Optimal power flow: a bibliographic survey i. *Energy Systems*, 3(3), 221–258.
- Gan, L., Li, N., Topcu, U., & Low, S. H. (2014). Exact convex relaxation of optimal power flow in radial networks. *IEEE Transactions on Automatic Control*,

- 60(1), 72–87.
- Gan, L., Topcu, U., & Low, S. H. (2012). Optimal decentralized protocol for electric vehicle charging. *IEEE Transactions on Power Systems*, 28(2), 940–951.
- Gopalakrishnan, A., Raghunathan, A. U., Nikovski, D., & Biegler, L. T. (2013). Global optimization of multi-period optimal power flow. In *2013 American Control Conference*, (pp. 1157–1164). IEEE.
- Guille, C. & Gross, G. (2009). A conceptual framework for the vehicle-to-grid (v2g) implementation. *Energy policy*, 37(11), 4379–4390.
- Huang, S., Wu, Q., Wang, J., & Zhao, H. (2016). A sufficient condition on convex relaxation of ac optimal power flow in distribution networks. *IEEE Transactions on Power Systems*, 32(2), 1359–1368.
- Hutson, C., Venayagamoorthy, G. K., & Corzine, K. A. (2008). Intelligent scheduling of hybrid and electric vehicle storage capacity in a parking lot for profit maximization in grid power transactions. In *2008 IEEE Energy 2030 Conference*, (pp. 1–8). IEEE.
- INSIDEEVs (2020). Nissan leaf: "the world's most popular ev with 450,000 sold since 2010. <https://insideevs.com/news/393890/nissan-leaf-sales-450000>.
- Jabr, R. A. (2006). Radial distribution load flow using conic programming. *IEEE transactions on power systems*, 21(3), 1458–1459.
- Jabr, R. A. (2011). Exploiting sparsity in sdp relaxations of the opf problem. *IEEE Transactions on Power Systems*, 27(2), 1138–1139.
- Jabr, R. A. (2014). Minimum loss operation of distribution networks with photovoltaic generation. *IET Renewable Power Generation*, 8(1), 33–44.
- Jabr, R. A., Coonick, A. H., & Cory, B. J. (2002). A primal-dual interior point method for optimal power flow dispatching. *IEEE Transactions on Power Systems*, 17(3), 654–662.
- Jolissaint, C. H., Arvanitidis, N., & Luenberger, D. G. (1972). Decomposition of real and reactive power flows: a method suited for on-line applications. *IEEE Transactions on Power Apparatus and Systems*, (2), 661–670.
- Judd, S. L. & Overbye, T. J. (2008). An evaluation of phev contributions to power system disturbances and economics. In *2008 40th North American Power Symposium*, (pp. 1–8). IEEE.
- Kempton, W. & Letendre, S. (1997). Electric vehicles as a new power source for electric utilities, transpn res. *D Transport and Environment*, 2, 157–175.
- Kempton, W. & Tomić, J. (2005). Vehicle-to-grid power fundamentals: Calculating capacity and net revenue. *Journal of power sources*, 144(1), 268–279.
- Kocuk, B., Dey, S. S., & Sun, X. A. (2016). Strong SOCP relaxations for the optimal power flow problem. *Oper. Res.*, 64(6), 1177–1196.
- Kocuk, B., Dey, S. S., & Sun, X. A. (2018). Matrix minor reformulation and SOCP-based spatial branch-and-cut method for the AC optimal power flow problem. *Math. Prog. Comp.*, 10(4), 557–596.
- Li, N., Gan, L., Chen, L., & Low, S. H. (2012). An optimization-based demand response in radial distribution networks. In *2012 IEEE Globecom Workshops*, (pp. 1474–1479). IEEE.
- Masoum, M. A., Moses, P. S., & Hajforoosh, S. (2012). Distribution transformer stress in smart grid with coordinated charging of plug-in electric vehicles. In *2012 IEEE PES Innovative Smart Grid Technologies (ISGT)*, (pp. 1–8). IEEE.
- Molzahn, D. K. & Hiskens, I. A. (2014). Moment-based relaxation of the optimal



- power flow problem. In *2014 Power Systems Computation Conference*, (pp. 1–7). IEEE.
- Molzahn, D. K., Holzer, J. T., Lesieutre, B. C., & DeMarco, C. L. (2013). Implementation of a large-scale optimal power flow solver based on semidefinite programming. *IEEE Transactions on Power Systems*, *28*(4), 3987–3998.
- Moyano, C. & Salgado, R. (2010). Adjusted optimal power flow solutions via parameterized formulation. *Electric power systems research*, *80*(9), 1018–1023.
- Nakawiro, W., Erlich, I., & Rueda, J. L. (2011). A novel optimization algorithm for optimal reactive power dispatch: A comparative study. In *2011 4th International Conference on Electric Utility Deregulation and Restructuring and Power Technologies (DRPT)*, (pp. 1555–1561). IEEE.
- NHTS (2017). 2017 national household travel survey by united states department of transportation, federal highway administration. <https://nhts.ornl.gov>.
- NISSAN (2020). Nissan leaf range batteries. <https://www.nissanusa.com/vehicles/electric-cars/leaf/features/range-charging-battery.html>.
- Ongsakul, W. & Tantimaporn, T. (2006). Optimal power flow by improved evolutionary programming. *Electric power components and systems*, *34*(1), 79–95.
- Ortega-Vazquez, M. A., Bouffard, F., & Silva, V. (2012). Electric vehicle aggregator/system operator coordination for charging scheduling and services procurement. *IEEE Transactions on Power Systems*, *28*(2), 1806–1815.
- Paranjothi, S. & Anburaja, K. (2002). Optimal power flow using refined genetic algorithm. *Electric Power Components and Systems*, *30*(10), 1055–1063.
- Roa-Sepulveda, C. & Pavez-Lazo, B. (2003). A solution to the optimal power flow using simulated annealing. *International journal of electrical power & energy systems*, *25*(1), 47–57.
- Saber, A. Y. & Venayagamoorthy, G. K. (2010). Intelligent unit commitment with vehicle-to-grid—a cost-emission optimization. *Journal of Power Sources*, *195*(3), 898–911.
- Santos, A. J. & Da Costa, G. (1995). Optimal-power-flow solution by newton’s method applied to an augmented lagrangian function. *IEE Proceedings-Generation, Transmission and Distribution*, *142*(1), 33–36.
- Sasson, A., Vilorio, F., & Aboites, F. (1973). Optimal load flow solution using the hessian matrix. *IEEE Transactions on Power Apparatus and Systems*, (1), 31–41.
- Schuller, A., Dietz, B., Flath, C. M., & Weinhardt, C. (2014). Charging strategies for battery electric vehicles: Economic benchmark and v2g potential. *IEEE Transactions on Power Systems*, *29*(5).
- Shen, C. & Laughton, M. (1969). Determination of optimum power-system operating conditions under constraints. In *Proceedings of the Institution of Electrical Engineers*, volume 116, (pp. 225–239). IET.
- Shi, Y., Tuan, H. D., Savkin, A. V., Duong, T. Q., & Poor, H. V. (2018). Model predictive control for smart grids with multiple electric-vehicle charging stations. *IEEE Transactions on Smart Grid*, *10*(2), 2127–2136.
- Shoultz, R. R. & Sun, D. (1982). Optimal power flow based upon pq decomposition. *IEEE Transactions on Power Apparatus and Systems*, (2), 397–405.
- Soliman, S. A.-H. & Mantawy, A.-A. H. (2011). *Modern optimization techniques with applications in electric power systems*. Springer Science & Business Media.

- Sortomme, E. & El-Sharkawi, M. A. (2010). Optimal charging strategies for unidirectional vehicle-to-grid. *IEEE Transactions on Smart Grid*, 2(1), 131–138.
- Sulaiman, M. H., Mustafa, Z., Mohamed, M. R., & Aliman, O. (2015). Using the gray wolf optimizer for solving optimal reactive power dispatch problem. *Applied Soft Computing*, 32, 286–292.
- Sun, A. & Phan, D. T. (2011). Some optimization models and techniques for electric power system short-term operations. *Wiley Encyclopedia of Operations Research and Management Science*, 1–17.
- Sun, D. I., Ashley, B., Brewer, B., Hughes, A., & Tinney, W. F. (1984). Optimal power flow by newton approach. *IEEE Transactions on Power Apparatus and systems*, (10), 2864–2880.
- Tang, W. & Zhang, Y. J. A. (2016). A model predictive control approach for low-complexity electric vehicle charging scheduling: Optimality and scalability. *IEEE transactions on power systems*, 32(2), 1050–1063.
- Tomić, J. & Kempton, W. (2007). Using fleets of electric-drive vehicles for grid support. *Journal of power sources*, 168(2), 459–468.
- Torres, G. L. & Quintana, V. H. (1998). An interior-point method for nonlinear optimal power flow using voltage rectangular coordinates. *IEEE transactions on Power Systems*, 13(4), 1211–1218.
- Valentine, K., Temple, W. G., & Zhang, K. M. (2011). Intelligent electric vehicle charging: Rethinking the valley-fill. *Journal of Power Sources*, 196(24), 10717–10726.
- Wang, J., Bharati, G. R., Paudyal, S., Ceylan, O., Bhattarai, B. P., & Myers, K. S. (2019). Coordinated electric vehicle charging with reactive power support to distribution grids. *IEEE Transactions on Industrial Informatics*, 15(1), 54–63.
- Yang, J., He, L., & Fu, S. (2014). An improved pso-based charging strategy of electric vehicles in electrical distribution grid. *Applied Energy*, 128, 82–92.
- Yang, Z., Li, K., & Foley, A. (2015). Computational scheduling methods for integrating plug-in electric vehicles with power systems: A review. *Renewable and Sustainable Energy Reviews*, 51, 396–416.
- Yang, Z., Li, K., Niu, Q., Xue, Y., & Foley, A. (2014). A self-learning tlbo based dynamic economic/environmental dispatch considering multiple plug-in electric vehicle loads. *Journal of Modern Power Systems and Clean Energy*, 2(4), 298–307.
- Yilmaz, M. & Krein, P. T. (2012). Review of the impact of vehicle-to-grid technologies on distribution systems and utility interfaces. *IEEE Transactions on power electronics*, 28(12), 5673–5689.
- Yuksel, T., Tamayao, M.-A. M., Hendrickson, C., Azevedo, I. M., & Michalek, J. J. (2016). Effect of regional grid mix, driving patterns and climate on the comparative carbon footprint of gasoline and plug-in electric vehicles in the united states. *Environmental Research Letters*, 11(4), 044007.
- Zakariazadeh, A., Jadid, S., & Siano, P. (2014). Multi-objective scheduling of electric vehicles in smart distribution system. *Energy Conversion and Management*, 79, 43–53.
- Zhang, J., Yigang, H., Mingjian, C., & Yongling, L. (2017). Primal dual interior point dynamic programming for coordinated charging of electric vehicles. *Journal of Modern Power Systems and Clean Energy*, 5(6), 1004–1015.